Physics – Uspekhi **68** (8) 759 – 784 (2025)

CONFERENCES AND SYMPOSIA

PACS numbers: 52.40.Kh, **94.05. – a**

ON THE 100th ANNIVERSARY OF S.I. SYROVATSKII'S BIRTH

Thin and superthin current sheets: journey into the depths of Syrovatskii's singularity *

L.M. Zelenyi, H.V. Malova, E.E. Grigorenko, V.Yu. Popov, O.O. Tsareva, M.V. Leonenko

DOI: https://doi.org/10.3367/UFNe.2025.03.039950

Contents

Abstract. **We discuss the history of the study of thin (proton-thickness) current sheets in space plasma, which in the magnetohydrodynamic (MHD) framework were regarded as singular structures, i.e., infinitely thin MHD discontinuities. We discuss the special role of the work of S.I. Syrovatskii and his group in developing the theory and experimental studies of nonstationary thin current sheets in application to solar flares. Multisatellite scientific missions (Interball, Cluster, and MMS) have allowed looking inside the 'singularities' and evaluating the most complex processes of energy accumulation, transformation, and release within them. The accumulation of observational data from multisatellite space missions and the development of theoretical models of thin sheets allows their complex internal structure to be studied, including a hierarchical embedding of thinner current sheets inside thicker ones. Even in a not very thin sheet, the plasma dynamics can no longer be described within the MHD approximation and requires the motion of electrons and ions to be described separately, at least. Describing ions is especially challenging because of their large Larmor radius (possibly exceeding the sheet thickness). The so-called quasiadiabatic theory of the motion of charged particles in the presence of sharp magnetic gradients plays a major role here. We reveal the key role of thin embedded structures as triggers of explosive magnetic reconnection and conversion of the free energy of magnetic fields into the energy of waves and flows of accelerated particles. The relevant issue of observing and interpreting the properties of superthin (electron-scale) current sheets is covered in detail. Such sheets can be both part of multilevel embedded structures and multiple independent nonstationary formations related to the magnetic energy dissipation processes in hot collisionless**

L.M. Zelenyi [(1,a)], **H.V. Malova** [(1,2,b)], **E.E. Grigorenko** [(1,c)], **V.Yu. Popov** [(1,3,4,d)], **O.O. Tsareva** [(1,e)], **M.V. Leonenko** [(1,f)]
[(1)] Space Research Institute, Russian Academy of Sciences, ul. Profsoyuznaya 84/32, 117997 Moscow, Russian Federation
[(2)] Lomonosov Moscow State University, Skobeltsyn Institute of Nuclear Physics, Leninskie gory 1, str. 2, 119991 Moscow, Russian Federation
[(3)] Lomonosov Moscow State University, Faculty of Physics, Leninskie gory 1, str. 2, 119991 Moscow, Russian Federation
[(4)] HSE University, ul. Myasnitskaya 20, 101000 Moscow, Russian Federation
E-mail: [(a)] zelenyi@iki.rssi.ru, [(b)] hmalova@yandex.ru, [(c)] elenagrigorenko2003@yandex.ru, [(d)] popov@math380b.phys.msu.su, [(e)] olga8.92@mail.ru, [(f)] makarleonen@gmail.com

Received 20 June 2025
Uspekhi Fizicheskikh Nauk **195** (8) 807 – 834 (2025)
Translated by S. Alekseev

* The review is based on a talk given at the Scientific Session of the Physical Sciences Division of the Russian Academy of Sciences on 5 March 2025 (see *Phys. Usp.* **68** (8) 745 (2025); *Usp. Fiz. Nauk* **195** (8) 793 (2005)).

magnetospheric plasmas. The rapid evolution and decay of these sheets lead to the acceleration of electrons and the formation of new sheets, which also decay and give rise to new thin current structures; therefore, reconnection does occur on the electron scale, albeit in a nontrivial cascade mode. Several decades have passed since Syrovatskii constructed the MHD model of a dynamical current sheet, and the experience of improving both experimental techniques and theoretical tools that have allowed looking inside these amazing structures is instructive.

Keywords: collisionless cosmic plasma, thin current sheets, metastability, magnetic reconnection, superthin electron sheets, electron tearing mode, cascade reconnection

1. Introduction

1.1 Current sheets in space: stationary or dynamical? Dilemma: neutral sheet or Petschek current

Since the 1960s, much attention of the scientific community of space physicists has been focused on the heated debate between proponents of stationary reconnection models [1–4] and dynamical current sheets (CSs) [5–7]. During that time, ground-based and satellite observations have revealed the critical role of CSs in converting the magnetic energy stored in them into the thermal and kinetic energy of plasma. The processes of solar flares as well as various processes occurring during geomagnetic disturbances had to be explained (here and hereafter, we discuss the most studied and uniquely interpretable manifestations of geomagnetic substorms, such as auroras and precipitation of energetic particle flows in the tail and the auroral region). The celebrated American scientist Charles Kennell wrote an article [8] about the interpretation of the obtained data from the standpoint of the resistivity of collisionless plasma in space, called "What we have learned from the magnetosphere." There, he identified three new physical phenomena that many space physicists had been unaware of: collisionless shock waves, the interaction of waves with particles, and reconnection. The specificity of these problems in Kennell's formulation was determined by the fact that space plasma is, in principle, practically collisionless and has no resistive dissipation, and therefore the problem had to be solved in some very complicated way in the absence of resistivity. In his studies [9, 10] and oral statements, the classic MHD scientist Hannes Alfvén expressed a negative attitude toward this problem, asserting that no magnetic reconnection can occur and magnetic field lines are also questionable; he ultimately rejected the formulation of the problem of reconnection as incorrect.

At the same time, another group of scientists can be singled out who adhered to the opposite standpoint and expressed ideas about the possibility of reconnection of magnetic field lines (see, e.g., [11]). By the 1960s, breakthrough ideas [12, 13] were formulated to explain the mechanism of instability of Earth's magnetospheric tail and the mechanism of excitation of magnetic storms and substorms. It was precisely in the 1960s–1970s that the Soviet scientist Sergei Ivanovich Syrovatskii also studied this topic and produced a number of remarkable studies on the dynamics of CSs [5–7, 14, 15]. The ideas that Syrovatskii consistently developed amount to the formation of a nonstationary CS, which was necessary to explain solar flare activity, the ejection of accelerated plasma, and the restructuring of magnetic fields after flares in the photosphere and corona.

In a parallel development, many scientists in the West also began to take an active interest in reconnection processes. The principal question was how to quickly 'disrupt' and reconnect magnetic fields in a collisionless plasma by changing their topology. It is known that disrupting magnetic field lines requires a dissipative violation or a violation of the freezing-in condition, which means that the plasma must be conductive in the region of the magnetic field disruption. Different models with various magnetic configurations were proposed, and scientists took various physical factors into account that could enhance the reconnection rate.

The simplest model of the stationary (forced) process of reconnection (annihilation) of magnetic fields in space plasma was proposed by Parker and Sweet [1–3]: plasma with a frozen-in magnetic field $\mathbf{B}_0$ under the action of an electric field $\mathbf{E}$ transferred field lines with a velocity $\mathbf{u} \sim \mathbf{E} \times \mathbf{B}_0$ to a special point X on both sides of which the magnetic fields $\mathbf{B}_0$ were pointing in opposite directions. The basic scheme of the Parker–Sweet model is shown in Fig. 1a. In a small neighborhood of the diffusion region (we call it the X-line), the freezing-in condition is violated, and the field lines break and reconnect, which is accompanied by a change in their topology. The energy stored in the magnetic field dissipates on the scale $l = L/\sqrt{\mathrm{Re_m}}$, where L is the sheet thickness and $\mathrm{Re_m}$ is the magnetic Reynolds number. The reconnection rate estimates in this model were small and did not agree with the observed high rates of spontaneous reconnection in chromospheric flares and powerful energy ejections.

Somewhat later, Petschek [4] proposed a more complex stationary model of forced reconnection, in which two pairs

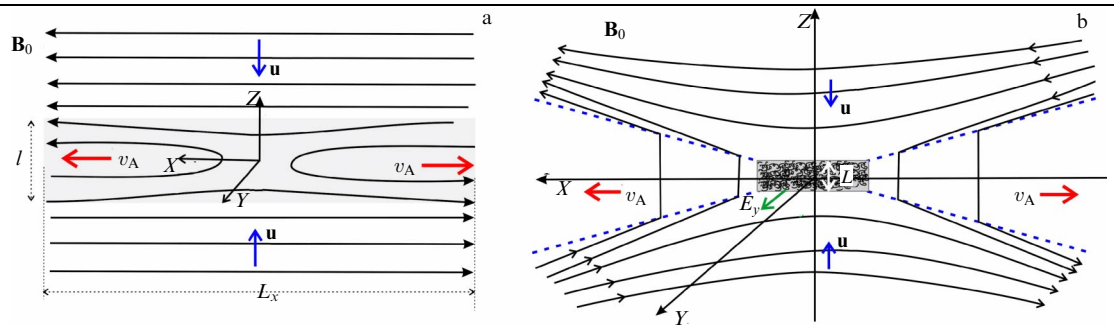

Figure 1. (a) Parker–Sweet and (b) Petschek models, represented in GSM coordinate system of magnetotail. X-axis is directed from Earth to Sun. Solid black lines show magnetic field lines entering reconnection region with velocity u (blue arrows) and leaving it after reconnection with Alfvén velocity (red arrows). Figure b shows direction of electric field E_y in reconnection zone and zone thickness L.

of stationary shock waves depart from the diffusion region around the X-line, as shown in Fig. 1b. Both models in Fig. 1 are shown in the standard geocentric solar-magnetospheric coordinate system (GSM), which is standardly used to describe the geomagnetic field. In it, the X-axis is directed from Earth to the Sun, the Y-axis from east to west, and the Z-axis along the geomagnetic dipole. A more detailed description of the coordinate system and its orientation relative to Earth's magnetosphere is given below. In Fig. 1, differently directed magnetic fields with plasma drift toward the X-line from above and from below. In the diffusion region, the field unfreezes, which is followed by reconnection of the magnetic field lines. The annihilation of the magnetic field is accompanied by energy dissipation into kinetic and thermal energy of the plasma. Standing shock waves ensure effective rotation, acceleration, and removal of the plasma on both sides of the X-line with a much higher velocity than in the Parker–Sweet model [1–3]. In the Petschek model, the reconnection rate M can be estimated as $M = u/v_A$, where u is the velocity of plasma inflow into the discontinuity region and v_A is the Alfvén velocity. The Petschek model with a higher reconnection rate turned out to be very attractive for explaining various processes in cosmic plasma, specifically, the release of large amounts of energy over short time intervals in cosmic flares. However, it was found later that the reconnection rates in the Petschek model are still insufficient to explain the observed flares and other processes. This was especially noticeable in numerical modeling of reconnection processes in collisionless plasma, which has low resistivity. To provide the required reconnection rate, anomalous resistance, turbulence, and various kinetic effects had to be taken into account [16, 17].

But it turned out that, in Petschek's model of magnetic reconnection, in a dissipative region of small size, the reconnection rate was still not high enough to provide the high rate observed in experiment. Petschek's model began to be modified in various ways, taking resistive mechanisms into account to increase the rate [16–20]. Gradually, it became clear that stationary models cannot in principle describe the explosive processes of spontaneous magnetic reconnection occurring in space plasma accompanied by pulsed energy release processes. The processes occurring in space are fundamentally nonstationary: following the formation and evolution of a CS, a disruption phase inevitably occurs, accompanied by magnetic reconnection, which can proceed sufficiently close to Petschek's description only in some very idealized cases.

An alternative to Petschek's standpoint on reconnection processes was provided by Syrovatskii's model [5–7, 14, 15]. It was due to Syrovatskii's school that the idea was introduced into scientific circulation that the evolution of plasma flows in highly conductive plasma within MHD must necessarily lead to the formation of CSs in the form of nonstationary singular current structures [19–21]. Syrovatskii was the first to understand and describe the role of CSs in accumulating magnetic energy. To explain the evolution of magnetic loops in the solar corona, flare processes, and energy release, he constructed a fairly simple analytic model in the approximation of a strong magnetic field, where center stage was taken by a variable-length CS in the form of a flat discontinuity surface separating magnetic fields of opposite directions. Using this simple model, the magnetic energy stored by the sheet was calculated using the

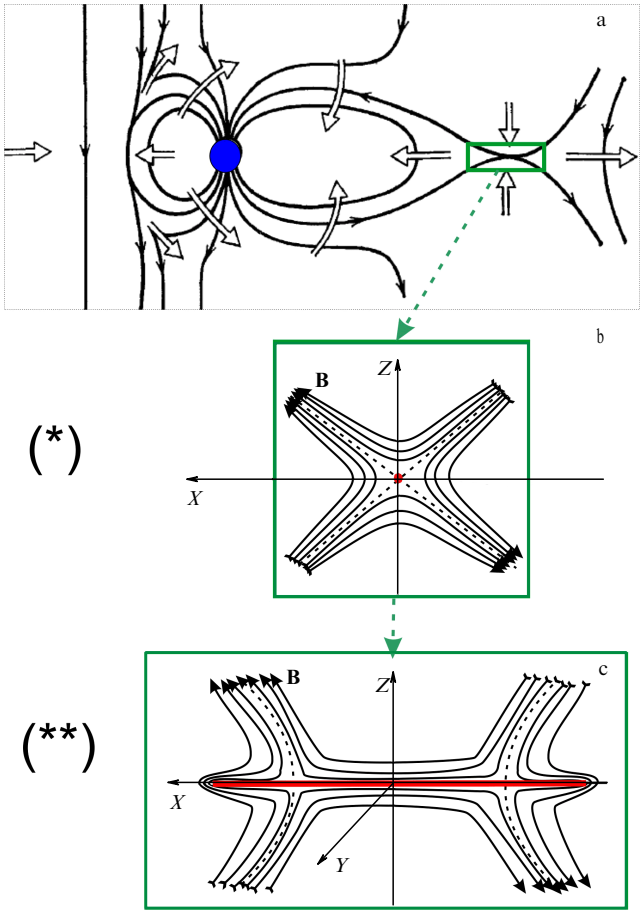

Figure 2. Dungey model of magnetosphere evolution [12] during geomagnetic disturbance. (a) Wide hollow arrows show motion of magnetic field lines: reconnection on day side, their transfer to night side, and thinning of CS tail with formation of X-line (CS is highlighted by green rectangle; center of X-line is marked by red dot in Fig. b). Schematically shown are (b) structure of X-line formed by magnetic field lines (**B**) at initial instant (*) and (c) development of Syrovatskii's CS (shown in red) at subsequent instants of time (**). Figure also shows GSM coordinate system mentioned in text.

straightforward formula [20]

$$w = \int (B^2 - h_0^2 r^2)\,\frac{\mathrm{d}V}{8\pi} = \frac{h_0^2 b^4}{32}\left(\ln\frac{4l^2}{b^2} - \frac{1}{2}\right) = \frac{LJ^2}{2c^2},$$

where B is the magnetic field strength on both sides of the sheet, h_0 is the gradient of the external magnetic field near the zero line, r is the coordinate along the sheet, b is the half-width of the current sheet, J is the surface current in the sheet, l is the characteristic size of the contour that closes the current in the sheet, and c is the speed of light. When the system accumulates energy, the CS becomes thinner, and therefore the current increases, causing the sheet to expand in the plane of the current and the energy in it to grow.

Figure 2 schematically shows characteristic configurations of the Syrovatskii model at two points in time: (*) at the beginning of the emergence of an X-point, and (**) during the development of the CS and its evolution.

In the Syrovatskii model, the reconnection process occurs in a neutral CS and has a dynamical nonstationary nature. At the initial time instant (*), shown in Fig. 2, a magnetic field configuration with an X-point forms, similar to the one in the

Petschek model. The plasma drift flow arising under the action of the electric and magnetic fields is directed toward the neutral line and has a cumulative nature, i.e., accumulates in the vicinity of the line. The magnetic field flux frozen into the plasma in the vicinity of the X-point does not have enough time to unfreeze and reconnect and becomes denser, and therefore magnetic energy accumulation begins in this region, in accordance with (1) in [20]. As a consequence, the CS narrows in the Z direction and lengthens along the X coordinate (Fig. 2, instant (**)). According to Syrovatskii's model, the CS elongation in the X direction occurs until the sheet ruptures under the influence of the so-called tearing instability, when the excess magnetic energy stored in the sheet is transformed into the energy of acceleration and heating of plasma particles. The powerful induction electric fields that arise when the sheet ruptures have a pulsed nature. Under their action, plasma particles can be rapidly accelerated to high energies in a short time. As it turned out, just Syrovatskii's nonstationary model, despite its rather significant simplifying assumptions, agrees well with the data from observations of flares in the solar corona and direct measurements by spacecraft of magnetic disturbances in the tail of Earth's magnetosphere [20, 22–25].

We note that the validity of this model was brilliantly confirmed in laboratory experiments and studies begun in the 1970s by Syrovatskii at the Lebedev Physical Institute of the Russian Academy of Sciences and continuing to this day in the laboratory of the Prokhorov General Physics Institute of the Russian Academy of Sciences (formerly a division of the Lebedev Physical Institute) under the supervision of Anna Frank [25]. A cumulative plasma flow leading to a configuration with a neutral CS was reproduced in laboratory conditions, and the mechanisms of instability development and destruction of the CS, accompanied by strong pulsed electric fields and acceleration of charged particles, were studied in depth. To adapt the model to galactic and stellar systems, modifications were proposed in which the reconnection rate was even faster than in the original formulation [21, 25–30].

1.2 Syrovatskii's dynamical current sheet as a solution to problem of solar flares and reconnection processes in space

Despite the obvious advantage of Syrovatskii's nonstationary model, the dilemma of 'a neutral sheet or the Petschek flow' persisted in science for quite a long time. Only two decades after the start of the discussion about the neutral sheet, an eminent MHD expert, Biskamp, in his famous book *Nonlinear Magnetohydrodynamics* [31], compared in detail two alternative scientific schools studying MHD reconnection processes: the Western school of Petschek and the Eastern school of Syrovatskii, noting that Syrovatskii's theory gives a qualitatively correct picture of the processes occurring in space, although the model is over-idealized. A little later, Biskamp showed the incorrectness of the boundary conditions in Petschek's model [32, 33]. This important statement actually put an end to many years of debate about the priorities of scientific approaches. The development of Petschek's model turned out to be a dead end, and Syrovatskii's was successful and applicable to the description of natural phenomena.

Let us formulate the main achievements associated with Syrovatskii's model and its significance for modern space research:

(1) Syrovatskii was the first to understand and describe the role of CSs in collisionless plasma as an accumulator of magnetic energy, which can be accumulated and then spontaneously released;

(2) Syrovatskii's model helped clarify the question of how plasma flows in strong nonuniform magnetic fields contribute to the formation of neutral (current) sheets and how magnetic energy is concentrated in them, leading to instability;

(3) although formally the ideal MHD used in Syrovatskii's model would have led to the formation of a singular surface, he noted that the development of tearing instabilities known at that time (collisionless or resistive) would ultimately lead to spontaneous destruction of the CS and flare phenomena, with the energy of the annihilating magnetic field transformed into plasma energy;

(4) the processes of rapid restructuring of magnetic fields in the regions of solar flares, the emergence of accelerated particles and solar cosmic rays, and the generation of cosmic rays in supernovae, galactic nuclei, and quasars were explained [34].

Eventually, the importance of taking kinetic effects in plasma into account became clear, which facilitated further research into the inner structure and dynamics of thin CSs in space [35], which were already regarded as infinitely thin MHD discontinuities, or singularities, in the 1960s. At that time, there was a joke among theorists developing plasma models in various approximations "MHD against the kinetics is like a carpenter against a cabinetmaker...."

To summarize the historical digression, we note that the pressing question posed at the time about the need to resolve the reconnection dilemma and to choose between a neutral sheet [5, 6] or the Petschek flow [4] in the vicinity of the diffusion region has been definitively resolved from the standpoint of observations *in situ* by modern high-resolution space missions in favor of research based on the ideas of cumulative energy accumulation, nonstationary magnetic reconnection in CSs, and the transformation of magnetic energy into the kinetic and thermal energy of plasma particles, developed by Syrovatskii and his students. These ideas largely determined the development of not only theoretical models but also general concepts about the most complex processes in space occurring at different scales in the Universe, from Earth's magnetosphere and heliosphere to the astrospheres of stars and galactic magnetic fields [16, 20, 21, 25, 29, 30].

2. Structure and dynamical properties of extremely thin current sheets in cosmic plasma

2.1 Ion current sheets: detection and properties

In 1962, based on experimental observations of the geomagnetic field, Ness [36] described the shape of Earth's magnetosphere as a magnetic dipole strongly compressed on the day side and a nondipole magnetic structure strongly elongated on the night side, resembling a comet tail streamlined by the solar wind (SW). A schematic cross section of the magnetosphere is shown in Fig. 3. The magnetospheric structure elongated on the night side of Earth is called the magnetotail. It stretches due to the quasiviscous interaction of the SW flow with Earth's dipole magnetic field, as shown in the figure. The symmetry plane of the tail contains a flat CS, where a current of density J_y flows from the morning to the evening side, self-consistently maintaining differently direc-

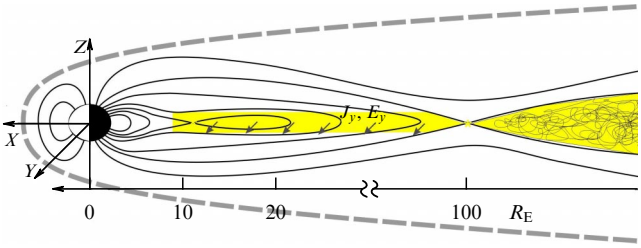

Figure 3. Schematic representation of Earth's magnetosphere and GSM coordinate system used to describe it. Lower axis shows approximate distances in tail, up to $100R_E$, where distant X-line is located. At distances of approximately $(12–15)R_E$, magnetic reconnection can occur during substorms with formation of a closed plasmoid. Typical for distances longer than $100R_E$ are strong turbulence of electromagnetic field, significant weakening of normal magnetic B_z component, and its chaotic oscillations. On distant neutral line, reverse process of disconnection of SW from geomagnetic field occurs. Gray dashed line indicates magnetopause — boundary separating planet magnetosphere from SW. In equatorial plane of tail, arrows show directions of large-scale electric field and current density.

ted magnetic fields in the northern and southern magnetosphere lobes (see, e.g., review [35]), and a large-scale electric field E_y is also observed. The CS thickness under quiet conditions ranges from one to several Earth radii R_E ($R_E \approx 6400$ km). The normal component of the magnetic field, that is due to the elongated dipole field, exists in the magnetotail CS up to distances of more than $100R_E$, which is the region of the distant neutral line where the SW lines thrown into the tail and reconnected by the geomagnetic field are disconnected from the magnetosphere and are carried away into the SW. In the region beyond the distant neutral line, the normal magnetic component weakens and becomes comparable to the fluctuation level [35, 37]. Figure 3 also shows the GSM coordinate system whose X-axis is directed from the center of Earth to the Sun, the Z-axis is along the geomagnetic dipole to the north, and the Y-axis is from morning to evening.

During geomagnetic disturbances at distances of the order of $(10–15)R_E$, an X-line can form in the magnetotail, leading to magnetic reconnection and the emergence of (one or more) plasmoids, i.e., magnetic islands with plasma, also shown in Fig. 3. After the discovery of the magnetotail, it remained unclear for quite a long time (several decades) where exactly and in what form the mechanisms that ensure the spontaneous development of energy release processes in the magnetosphere and large-scale disturbances of the geomagnetic field are realized. The development of theoretical models and ideas about the dynamics of the magnetosphere during interaction with the SW [12, 13, 38] allowed estimating the amount of energy coming from it into the magnetosphere before geomagnetic disturbances (of the order of 10^{24} erg), and the study of specific mechanisms of dissipation of the magnetospheric energy and its transformation into thermal and kinetic energy of plasma flows began [39–41].

In the 1990s, two main scenarios of energy accumulation and release were considered and discussed in studying geomagnetic disturbances: (1) direct energy release and (2) indirect energy release after injection into the magnetosphere [42–44]. Direct energy release begins almost immediately after the start of its accumulation in the magnetosphere. Indirect release occurs after some delay (the so-called substorm growth or preparation phase), which lasts from 30 min to 2 h, and sometimes more. Note that the energy release occurs quickly, taking a much shorter time than the accumulation phase. Accordingly, the process of explosive onset of a substorm in the magnetosphere is called the explosive phase. Once again, we note that, by magnetospheric disturbances, we primarily mean magnetospheric substorms, which are relatively weak geomagnetic disturbances and hence are the easiest to interpret. Magnetic storms release much more energy, and the energy release process can have very complex dynamics, which would be difficult to explain. However, we note that the mechanisms underlying substorm/storm activations and energy dissipation have a common nature: energy accumulation → magnetic reconnection → energy transformation → subsequent dissipation of energy. Schematically, two scenarios of the process of energy accumulation and release as a function of time are shown in Fig. 4 a, b.

According to observational data, the second scenario of energy transformation (Fig. 4b) is realized in the magnetosphere more often than the first. The second scenario allows an analogy with solar flares to be drawn. It first corresponds to the energy accumulation period [45]. At the initial stage, a small dissipation can occur, but later a sharp explosive release of energy occurs, both in solar flares and in the geomagnetic

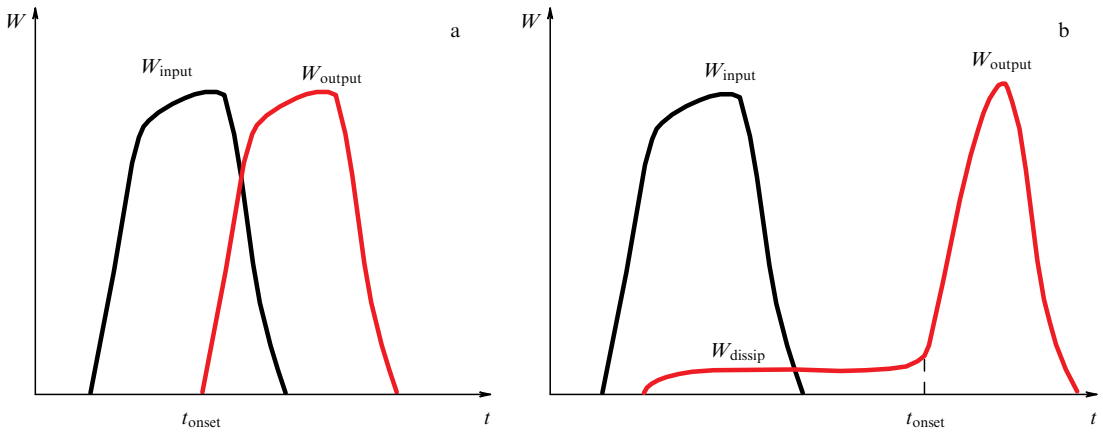

Figure 4. Two scenarios of accumulation of energy W_{input} in magnetosphere and release of energy W_{output} in Earth's magnetosphere: (a) direct and (b) indirect. In second scenario, dissipative energy W_{dissip} is released during energy input into magnetosphere, and (explosive) onset of the substorm can occur at instant t_{onset} much later than energy W_{input} enters system.

tail during magnetic substorms. Similar phenomena of energy accumulation and spontaneous explosive release were also registered in laboratory experiments. The primary objective was to understand the nature of this metastability and explain it. However, this turned out to be impossible in the MHD framework. The question of what kind of magnetospheric structure in a collisionless plasma can accumulate such large amounts of energy and then spontaneously and quickly release them arose before researchers with all its urgency.

In the 1990s, along with theoretical approaches, space observations began to actively develop. In particular, the domestic multisatellite project Interball was launched and operated in 1995–2000 [46]. Interball consisted of two satellite pairs positioned quite far from each other, in the outer and polar regions of the magnetosphere. With their help, new interesting results were obtained concerning plasma convection and substorm dynamics in Earth's magnetosphere [47]. As early as the late 1980s and early 1990s, thin CSs (TCSs) were discovered in the near part of Earth's magnetotail: they were flat, practically one-dimensional, current structures about one to several proton gyroradii in thickness [52–61]. For example, data from two closely located ISEE1 and ISEE2 spacecraft allowed detecting a TCS with a thickness of $0.2R_E$ (where $R_E \approx 6400$ km is Earth's radius) located inside a wider plasma sheet of the tail with a thickness of several R_E [57, 59]. Such current structures were typically detected in the magnetotail in the preparatory phase of a substorm and also in its distant part at distances longer than $(100–150)R_E$ from Earth [62]. Sometimes, the TCS thicknesses were even less than a proton gyroradius. These discoveries aroused great interest within the international scientific community and largely determined the launch of multisatellite missions in the 2000s [48, 63], whose purpose was to study local and global dynamical processes in Earth's magnetosphere.

Several multisatellite projects have played an important role. The first was the Cluster project. This mission, launched by the European Space Agency in 2000, made a major breakthrough in satellite-based CS research. The Cluster mission consisted of four satellites with an identical set of scientific instruments [48]. Near the orbital apogee, the satellites formed a tetrahedral configuration, which was maintained with fairly good accuracy. Thanks to four-point measurements of the magnetic field in three orthogonal planes, it was possible for the first time to calculate the magnetic field curl and determine the electric current density vector. Sufficiently fast CS crossings by the Cluster quartet allowed measuring the spatial profile of the current density in the direction normal to the sheet and studying its shape. The spatial separation of the satellites varied from several hundred to approximately 10,000 km, making it possible to record and study ion-scale CSs (e.g., [49, 50]). However, the distances separating the Cluster satellites did not allow observing CSs with thicknesses of less than a proton gyroradius, much less studying their spatial structure. In 2007, a mission of five THEMIS spacecraft (a NASA project) was launched to study manifestations of magnetospheric substorms, including the study of CSs, in different regions of the magnetosphere and at different distances from Earth. Later, this mission continued its research under the name ARTEMIS, and it helped to obtain interesting results on plasma-magnetic processes at the level of Moon's orbit. Somewhat later, in 2015, an American project similar to Cluster, Magnetospheric Multiscale (MMS), was launched, ideologically repeating the Cluster satellite configuration, but with tens of times smaller distances between the satellites. The MMS satellites for the first time observed and studied superthin CSs (STCSs) in detail, only a few gyroradii of thermal electrons in thickness, and even less in some cases [51]. We discuss the results of these studies in Section 4.

Importantly, multiscale configurations with embedded TCSs were observed not only in Earth's magnetotail [52–61] but also at the magnetopause, at the bow shock, in the SW [64–66], and in the magnetospheres of other Solar system planets: Mercury, Mars, and Jupiter [67–70]. In [71, 72], the different forms of observed TCS profiles were classified. It was noted in [73, 74] that TCSs are characterized by noticeable negative diamagnetic 'wings' of the current density at the sheet edges, caused by diamagnetic drift currents of quasi-trapped plasma near the particle demagnetization region. The markers of drift currents were local maxima on the magnetic field profiles (overshoots), framing the main current maximum in the CS center. CSs with asymmetric profiles have also been detected [71], possibly related to the asymmetry of plasma sources and/or asymmetry of plasma particle scattering in TCSs in the presence of the shear magnetic component B_y (see, e.g., [35, 75–77] and the references therein). It has been shown that TCSs are characterized not only by bell-shaped or peaked current density profiles but also by two- and three-peaked distributions [71, 35]. Space missions have shown the existence of bifurcated (splitted) TCSs, asymmetric and multiscale sheets with an intense TCS near the neutral plane, embedded in a thicker sheet with a lower current density [61, 71, 72]. All observations pointed to the universal nature of the physical mechanisms responsible for the self-consistent formation of TCSs.

Figure 5 (adapted from [71, 72]) schematically shows the characteristic generalized current density profiles with one, two, and three maxima observed by the Cluster satellites in Earth's magnetotail during magnetic substorms. An explanation for the observed diversity of fine current structures was proposed within the framework of many developing analytic and numerical models (see, for example, the review [35]). However, the most systematic approach to explaining the diversity of the magnetic field and current density profiles was developed within the kinetic model of an ion CS, inside which an even thinner electron sheet is embedded [78, 79]. The results of this model were supplemented and confirmed by numerical modeling [77, 80]. The concepts that were shaped about the structure of fine current structures became the first successful incursions of theoretical thought into tangential discontinuities, which the TCSs were believed to be from the standpoint of the MHD theory then dominant in space physics [31–33, 81–83]. Modifications of the analytic model taking magnetic shear components of different origins into account allowed even deeper insights, with the magnetic shear taken into account, into the internal structure of thin sheets, which were considered rotational discontinuities in MHD theory [76, 77, 84].

Thus, with the development of theoretical concepts based on observational data, TCSs in space plasma ceased to look like infinitely thin discontinuities to researchers, but 'acquired' a finite thickness. One- and two-dimensional models of TCSs began to be actively developed [35, 78, 79, 85–88]. In particular, to study the stability of CSs, researchers used Harris's simple and convenient analytic model [89], to which they non-self-consistently added a spatially constant normal magnetic component B_z [45, 90]. However, as we show in more detail in Section 3.4, such a model is

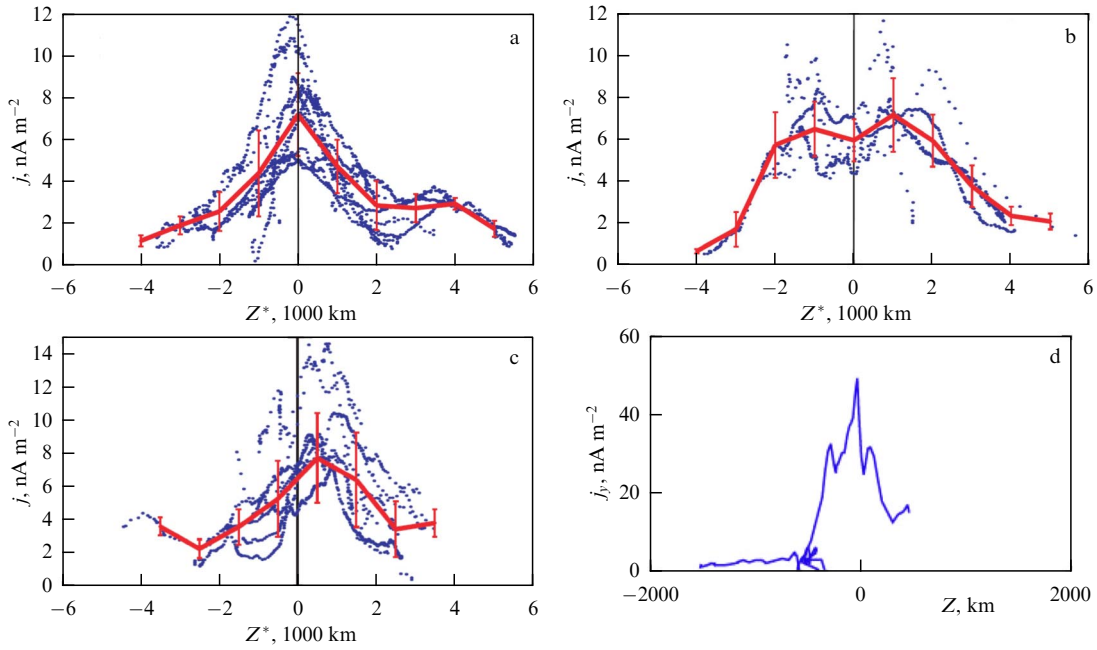

Figure 5. Varieties of observed current density profiles recorded by Cluster satellites in tail of Earth's magnetosphere: (a) with one maximum, (b) with two maximums, (c) asymmetric (adapted from [71]), and (d) with three maximums (adapted from [72]). Red curves in (a)–(c) show current density profiles averaged over observational data.

unsuitable for describing the stability of TCSs (see reviews [91, 92]); the range of its application gradually narrowed, mainly to problems of particle tracing in a given field (see, e.g., [93]).

In the early 2000s, self-consistent analytic models of TCSs were constructed [78, 79, 94, 95], and numerical self-consistent models were developed [77, 80]. Due to new observational data in the magnetotail, the Tsyganenko-89 empirical model, which was widely used in space physics but which had not previously allowed the magnetosphere on the night side far from Earth to be described, was modified by taking the CS of the magnetotail into account, which significantly expanded the scope of its application [96]. The role of TCSs as energy reservoirs capable of storing and releasing SW energy became clear [35, 63, 91, 92, 97, 98]. We note that almost all TCSs detected in the magnetotail were observed at the stage of substorm preparation; their configurations necessarily included a magnetic field component normal to the sheet, which is characteristic of the tail. Such CSs were supported by plasma flowing in from both sides with pronounced ion flow anisotropy (see, e.g., [72], detailed reviews [35, 67, 91], and the references therein).

The main properties of TCSs according to observations by the Cluster satellites [24, 26, 49, 71, 72] are given below (for clarity, the main points are highlighted in bold).

(1) A TCS has a **small thickness** $L \sim \rho_i \sim 250$–1000 km (where ρ_i is the ion gyroradius) and a high current density of ~ 10 nA m^{-2}. The field lines are very elongated: the ratio of the normal magnetic component to the tangential one is approximately $1/10$.

(2) The dominant current carriers, due to the significant temperature difference $T_i/T_e \geqslant 5$, are usually **ions** [55–57] in unclosed orbits [55, 99, 100], while, in the widespread sheet model [89], ions and electrons make comparable contributions to the current density.

(3) The current density profile is **embedded** inside a thicker plasma density profile [22, 59].

(4) The plasma flows feeding a TCS can have **flow anisotropy**, ranging from strong to moderate and weak. The internal structure of the TCSs and hence the observed profiles of characteristic quantities depend on this value [35, 101].

(5) Measurements by the Cluster satellites [24, 49, 63, 102] in the near-Earth magnetotail region ($\sim (15$–$20)R_E$) recorded both **non-splitted and splitted (bifurcated) current density profiles** (with one, two, and three current density maxima in the center of the sheet) [71, 72]. This distinguishes this type of CS from the model in [89], where protons and electrons together maintain the same bell-shaped plasma density profile with one maximum, coinciding in spatial scale with the current density distribution.

(6) During TCS observations, **symmetric and asymmetric** current density profiles relative to the neutral plane $z = 0$ can be encountered. The causes for this asymmetry have not yet been precisely determined [71, 103], although the model can provide a tentative answer to this question [104–106].

(7) A TCS exhibits metastability: it can be **stable for a long time** (from 15 min to 2 h) during the initial phase of a substorm, but **various instabilities can develop** in it later, leading to vertical oscillations (flapping) of the sheet, the occurrence of turbulence and, ultimately, to a rupture of the sheet and pinching of current filaments with the formation of magnetic islands. These phenomena invariably accompany magnetospheric disturbances and magnetic substorms and storms [91, 92, 98, 107–109].

2.2 Nature of metastability. Clash of ideas requiring construction of new class of thin current sheet models

It was noted in Section 2.1 that the formation of a TCS can be accompanied by its subsequent evolution and, ultimately, the development of a tearing mode in it, which can spontaneously develop and destroy the sheet. As shown in [35, 45, 91, 97, 110], the destruction of the sheet and magnetic reconnection in it are the most important processes initiating the explosive phase of a magnetospheric substorm. During the explosive

phase, the magnetic field energy accumulated in the tail is converted into the kinetic and thermal energy of plasma flows (see, e.g., [111–114]). Interestingly, in a TCS, the ions are demagnetized and move along characteristic quasiadiabatic trajectories, while the electrons, on the contrary, are magnetized. Below, we show that this difference in the dynamics of current-carrying particles is an important factor determining the metastability of the sheet.

The first CS models in the tail traditionally used the one-dimensional Harris current equilibrium model [89], which is mathematically simple and convenient for analytic calculations: the only tangential component of the magnetic field $B_x(z)$ changes sign, vanishing in the TCS neutral plane. Thus, in the GSM coordinate system (see Fig. 3), the profile of the magnetic tangential component is given by $B_x(z) = B_0 \tanh(z/L)$ (where L is the CS thickness and B_0 is the magnetic field at its edges), and the current and plasma density profiles are described by the respective expressions $j_y(z) = j_0/\cosh^2(z/L)$ and $n_{e,i}(z) = n_{0e,i}/\cosh^2(z/L)$ (where j_0 and $n_{0e,i}$ are the current density and the density of protons (i) or electrons (e) in the center of the sheet).

The most suitable candidate to play the role of a substorm trigger is arguably the tearing mode, which results in the sheet being torn and broken into current filaments, and a chain of magnetic islands forming in the magnetosphere tail (see Figs 2 and 3). However, at the beginning of the studies of geomagnetic disturbances, the main issue in considering the tearing instability was that the mechanisms of violating the freezing-in condition in collisionless plasma were practically unknown, and without taking them into account the processes of spontaneous or forced reconnection were impossible.

Landau damping of the tearing wave on electrons was proposed as the dissipative mechanism [115, 116]. In 1974, a similar concept was refined in [90], where the weak normal component of the magnetic field B_z, present in the tail, was taken into account. It turned out that an arbitrarily small normal component of the magnetic field B_z entirely destroys the Landau damping on electrons, but has little effect on the ion mode. It was also found that the magnetic component B_z, which magnetizes electrons [97], contributes to the so-called electron compressibility effect, which strongly stabilizes the instability in the system [117] because the excess free energy accumulated in the TCS is spent on compression/rarefaction of the magnetized electron component when a tearing wave passes through the system. This effect is very strong: it makes the CS almost totally stable against discontinuous disturbances in the magnetotail [131]. Thus, the idea of the electron tearing mode as a trigger for reconnection in the CS shifted toward the ion tearing mode.

The concept of total tail stability derived in this way, however, contradicted experimental observations. In the course of heated debates on this topic, it was shown in 1976 [97] that the discovered electron compressibility effect leaves narrow gaps in the parameter space where instability development is possible. The result obtained was in good agreement with the scenario of a magnetospheric substorm in the case of a metastable CS, in which the instability develops during the energy accumulation phase, leading to a rupture.

Subsequent refinements revealed that the electron compressibility effect can be strong in some configurations (see, e.g., reviews [35, 45, 91]), and the efforts of theoreticians were aimed at overcoming the electron compressibility effect for two more decades. For this, various mechanisms were invoked, such as turbulence, pitch-angle diffusion of electrons on whistlers [110, 118, 119], stochastic effects [120, 121], wave disturbances [122, 123], taking the population of passing electrons in the CS into account [124, 125], combined instability [126], and many others. None of the proposed models could offer a physically understandable scenario for the process of accumulation and release of energy in the magnetospheric tail that would be consistent with observational data [127–130].

In [131], when discussing whether ion tearing exists at all, the authors asserted that studies of ion tearing instability had reached a dead end. Studies [90, 117] actually completed the long-term discussion by concluding that the Harris model [89] used for theoretical analysis, with the nonzero normal component taken into account, was not suitable for describing the metastable CS of the magnetotail. Indeed, the non-self-consistent inclusion of the normal component of the magnetic field in the Harris model completely destroys this equilibrium and the magnetic topology in it [45]. The isotropy condition for the pressure tensor is also inapplicable to the description of thin current structures with a thickness of the order of the proton gyroradius [101]. It became clear that a suitable description of CSs with thicknesses of the order of proton gyroradii $L \sim \rho_i$ required creating a new kinetic (or hybrid) model, and pressure anisotropy had to be taken into account for equilibrium balance. At the same time, the question arose about the type of motion characteristic of plasma populations forming TCSs. In the next section, we consider the basic ideas about the structure of TCSs and the dynamics of particles in them.

The final answer turned out to be simpler than expected, and a hint arrived from an *in situ* experiment. The current profiles in current structures obtained by the Cluster satellite system [24] did not resemble simple Harris bell-shaped distributions [89, 132–135], but were narrow nested structures. Such sheets have much higher free energy than Harris sheets do, and this can be enough to overcome the stabilizing effect of electron compressibility. In Section 3, we detail both the TCS structure and the mechanisms of instability development in such CSs.

3. Inside the singularity: ion scale and creation of universal analytic theory of thin current sheets

3.1 Peculiarities of particle dynamics in magnetotail current sheet during geomagnetic disturbances

According to the generally accepted models of magnetospheric convection and the interaction of Earth's magnetosphere with the SW (see [12, 13] as well as Fig. 2), confirmed by observational data, in quiet geomagnetic conditions, that the magnetotail CS is a virtually isotropic plasma configuration such that the transverse (along z) scales of magnetic field variation are much larger than the proton gyroradius scales. Therefore, all plasma particles can be considered magnetized in quiet geomagnetic periods. Their drift currents form and self-consistently support the tail CS. The arrival of the southern IMF leads to active reconnection of magnetic field lines at the day magnetopause and the influx of SW energy into the magnetosphere. The increase in the magnetic flux in the magnetotail compresses the CS over a large area, approximately to the ionic thickness with the formation of a TCS, after which it can lose stability. Spontaneous develop-

ment of tearing instability leads to multiscale nonstationary processes of explosive magnetic reconnection in the tail, to the formation of magnetic islands (or ropes), and to increased plasma convection. The trigger for all these processes is the rupture of the thinned CS, which in the course of the compression process acquires totally new properties compared to the undisturbed state.

Because the TCS structure changes dramatically after compression, we briefly characterize the dynamics of charged particles in it, which should show the reasons for the formation of a spatial hierarchy of embedded like a matryoshka doll CSs inside the plasma sheet, that is the widest structure in comparison with TCS. Embedding and the possible presence of several peaks and depressions on plasma and current densities profiles are characteristic properties of a TCS, which are manifested not only in Earth's magnetosphere but also in planetary magnetospheres, the SW, and turbulent plasmas in space. Because the kinetic model is applicable to the description of the TCS structure, we start by considering the characteristic features of the motion of individual protons and electrons, which differ from the classical dynamics of particles whose motion is completely magnetized (i.e., completely controlled by the magnetic field). Such is, for example, the motion of plasma particles in the inner regions of the magnetosphere. To describe the unmagnetized motion of particles, when all the standard concepts associated with the guiding center approximation become inapplicable, a new quasiadiabatic theory [120] of particle motion was created (see review [135]) based on the approximate conservation of the action invariant I_z, first proposed by Sonnerup [134].

The motion of charged particles in a magnetic configuration with curved magnetic field lines is controlled by the adiabaticity parameter $\kappa = \sqrt{R_c/\rho_L}$, where R_c is the minimum curvature radius of the field lines and ρ_L is the maximum Larmor radius of the particle [35, 120, 135]. Particles with $\kappa > 1$ are magnetized, and their motion is completely controlled by the magnitude and direction of the magnetic field. Particles with $\kappa < 1$ are not completely controlled by it, their dynamics can be chaotic in the region κ less or about 1, and becomes quasi-adiabatic at $\kappa \ll 1$ [120, 135], which we discuss in more detail below.

The table illustrates the main characteristics of particle velocities and the pressures they support in the regions with $\kappa > 1$ and $\kappa < 1$. The left column characterizes the region $\kappa > 1$, where the guiding center approximation can be used to describe the particle motion: charged particles slide along magnetic field lines and simultaneously perform gyrorotation due to the Lorentz force. Their total velocity can be decomposed in a cylindrical coordinate system into components perpendicular and parallel to the magnetic field and the rotation phase φ. If there is no energy dissipation in the system, then the transverse and longitudinal invariants of motion, i.e., the magnetic moment μ and the longitudinal invariant J, are approximately conserved during the motion of such particles. The pressure tensor of magnetized plasma has a diagonal form, and the characteristic form of the tension balance is shown in the lower left column of the table. Because particles can scatter in plasma due to pitch-angle diffusion, the longitudinal velocity can transform and pass into the transverse velocity, which is also shown in the bottom row of the left column. We note that pitch-angle scattering does not change the general diagonal form of the stress tensor in the considered region of the adiabaticity parameter variation.

A different picture is observed for high-energy plasma particles, whose motion is weakly controlled by the magnetic field, with the adiabaticity parameter $\kappa < 1$. In the magnetotail TCS, the region of minimum curvature of magnetic field lines and maximum Larmor radii of particles falls on the neutral sheet, where the tangential component of the magnetic field reverses direction, $B_x(z \approx 0) \to 0$. As a consequence, upon entering the neutral sheet, the adiabaticity parameter decreases to values $\kappa < 1$. Depending on the particle energies, their gyrorotation can be superseded by chaotic dynamics, which is described within the framework of the quasiadiabatic theory [135]). Figure 6a shows three main characteristic trajectories of demagnetized protons in the vicinity of the TCS: transient, quasitrapped, and completely trapped [135–137].

At the sheet edges, the ion and electron fluxes are characterized by a flux anisotropy $\varepsilon = v_T/v_D$, where v_T and v_D are the thermal and drift velocities of the plasma particles. Higher-energy protons entering the neutral sheet can become transient [99, 100] and leave the CS after crossing it once. At the boundary of the neutral sheet, called the separatrix, they are demagnetized, and describe a semicircle in the field B_z, simultaneously performing fast vertical oscillations. Their trajectories in this region are called meandering, or serpentine. Having described a semicircle, the passing protons are magnetized again and leave the sheet. During the meandering motion, they carry elementary currents in the y direction and thus contribute to the total current. The main

Table. Comparison of main characteristics of charged particle motion and stress tensor in plasma for different values of adiabaticity parameter κ.

Adiabaticity parameter	$\kappa > 1$	$\kappa < 1$
Approximation	Guiding center	Quasiadiabatic
Particle velocity and coordinate system	$\mathbf{v} \to (v_\perp, v_\parallel, \varphi)$ Cylindrical coordinate system	$\mathbf{v} \to (v_0, \alpha_0, \beta_0)$ Spherical coordinate system
Motion invariants	$\mu = \dfrac{W_\perp}{B} \cong \text{const}$ $J = \dfrac{1}{2\pi}\oint v_\parallel \, \mathrm{d}l \cong \text{const}$	$I_z = \dfrac{1}{2\pi}\oint p_z \, \mathrm{d}z \cong \text{const}$ [99] $I_x = \dfrac{1}{2\pi}\oint p_x \, \mathrm{d}x \cong \text{const}$ [91, 120, 135]
Tension balance	$\rho \dfrac{\mathrm{d}\mathbf{v}}{\mathrm{d}t} = \dfrac{1}{c}[\mathbf{j} \times \mathbf{B}] - \nabla \begin{pmatrix} p_\perp & 0 & 0 \\ 0 & p_\perp & 0 \\ 0 & 0 & p_\parallel \end{pmatrix}$ $p_\parallel \to p_\perp$	$\rho \dfrac{\mathrm{d}\mathbf{v}}{\mathrm{d}t} = \dfrac{1}{c}[\mathbf{j} \times \mathbf{B}] - \nabla \begin{pmatrix} p_{xx} & p_{xy} & p_{xz} \\ p_{yx} & p_{yy} & p_{yz} \\ p_{zx} & p_{zy} & p_{zz} \end{pmatrix}$ $\dfrac{1}{c}[\mathbf{j} \times \mathbf{B}]_x = \dfrac{\mathrm{d}p_{xz}}{\mathrm{d}z}$

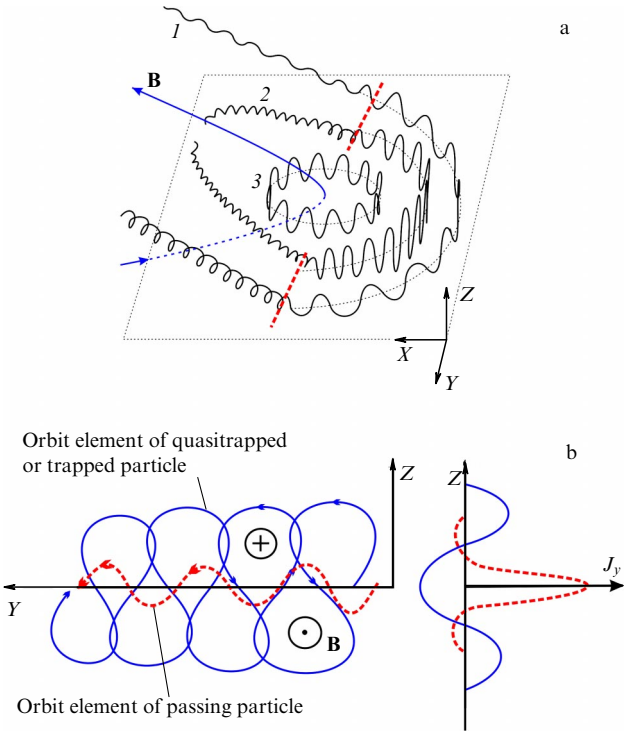

Figure 6. (a) Three possible types of trajectories in a TCS: open (*1*), quasiclosed (*2*), and completely captured (*3*) orbits (shown in GSM coordinate system). Plane of sheet is indicated by thin dotted line. Thick dashed red line denotes separatrices on which particle motion type changes from not crossing neutral sheet ($z = 0$) to crossing it. Blue line shows magnetic field line **B**. (b) Elements of quasiadiabatic orbits in neutral region: red dashed line corresponds to flyby orbit, and blue solid line, to captured or quasitrapped one. Current density profiles supported by particles are shown on right by respective dashed red and solid blue lines. Looping trajectories of quasitrapped particles in center of sheet have negative y velocities, and hence current density supported by them is negative in this region and positive at edges of sheet.

characteristic trajectories of the protons are shown in Fig. 6 together with the plasma density and current profiles they create.

Lower-energy quasitrapped ions are also demagnetized upon entering the sheet and describe a semicircle in the field B_z. At the exit from the TCS, they are captured by the magnetic field, drift in the negative y direction, and return to the CS (an example of such an orbit, also called a 'cucumber' orbit, is shown in Fig. 6a). The number of 'returns' is finite and depends on the ratio of the frequencies of fast and slow motions, but at some points in time protons can disperse with respect to the pitch angle, fly out of the TCS, and escape. Due to the closed trajectories, quasitrapped particles do not carry a current, although they can redistribute the profile of the main positive current. Due to their special dynamics, a negative local current can be observed in the neutral sheet in the symmetry plane of the sheet [132], which can be seen in Fig. 6.

The third type of orbit shown in Fig. 6 belongs to completely trapped particles not connected with the plasma flow entering the sheet. They are the lowest-energy particles, which move along quasiclosed (or completely closed) figure-eight or ring-shape orbits. They never cross the separatrix, and the total current carried by them is zero, as with quasitrapped particles. However, if the density of these particles is sufficiently high, they can participate in the redistribution of the total current, and their local currents, opposite to the main one, can be quite large.

Returning to the table, we focus attention on the right column, where the characteristics of the motion of particles with $\kappa < 1$ are shown from top to bottom. We note that the velocity of a particle during meandering motion can be represented in a spherical coordinate system in terms of the total velocity v_0 and the direction angles α_0 and β_0. Magnetic moments of such particles are not conserved, but the quasiadiabatic invariant of motion I_z, which is an analogue of the magnetic moment, is approximately conserved:

$$I_z = \oint p_z \, \mathrm{d}z \approx \mathrm{const}\,. \tag{1}$$

Here, p_z is the particle generalized momentum [120, 133–135]. In the neutral region of the TCS, the degrees of freedom along x and z 'decouple': slow rotation along the x coordinate is superimposed on fast oscillations along z, which can be seen in Fig. 6. When crossing the separatrices of motion, charged particles can experience small jumps of the quasiadiabatic invariant of motion ΔI_z. In the magnetotail, these jumps were estimated in [120] as

$$\Delta I_z \cong \mp \frac{3}{2}\,\kappa \sqrt{1 - I_z^{4/3}}\,\ln 2 |\cos\theta_{\mathrm{sep}}|\,, \tag{2}$$

where κ is the adiabaticity parameter and θ_{sep} is the particle phase when crossing the separatrix. For $\kappa \ll 1$, the jumps are much smaller than the invariant I_z itself: $\Delta I_z \ll I_z$ [35, 120, 135].

If a particle is quasitrapped and oscillates multiple times around the CS, then its longitudinal invariant I_x can also be conserved [88]. The motion of transient and quasitrapped particles with the approximate conservation of the invariant I_z in (1) was called quasiadiabatic. The tension tensor in a plasma with such particles is not gyrotropic, as in magnetized plasma, but anisotropic [101], as can be seen from a comparison of the left and right columns of the table.

It follows from the foregoing that the parameter κ plays a key role in the particle dynamics. For protons with $\kappa \ll 1$, the jumps in the invariants of motion upon entering the sheet are small compared to the values of the invariants themselves ($\Delta I_z \ll I_z$). Such ions mostly interact with the CS once and are transient; they are also the main current carriers in the y direction. In [120], their quasiadiabatic motion was first considered in detail and applied to the tail of Earth's magnetosphere. Based on this consideration, the TCS theory [78, 79, 94, 95] was developed and studied, using the approximate conservation of motion invariants. For ions with $\kappa \leqslant 1$, the jumps of the motion invariants ΔI_z at separatrix crossings can be significantly larger, and therefore their motion is considered chaotic, quasitrapped. For $\kappa \sim 1$–3 and especially for $\kappa > 3$ [120, 136, 137], the Larmor radii of the particles become significantly smaller than the magnetic inhomogeneity scale in the neutral sheet, and hence the motion of the particles is practically magnetized, and the guiding center approximation is applicable to their description [35].

3.2 Model of thin current sheets as new class of magnetoplasma equilibria. Estimation of characteristic thickness

After the discovery of the magnetotail, it was believed for a long time that a thick CS exists at low latitudes in the

equatorial region (with a characteristic scale much larger than the thermal ion gyroradii), supported by drift currents of magnetized plasma [138–140]. In analytic models describing such a 'thick' CS, the equilibrium between the magnetic field and plasma is maintained by plasma pressure gradients. Such models are usually two-dimensional [141]. In 1965, Speiser published a pioneering paper [99], where he suggested that the CS in the magnetotail is not always thick and can also be thin, and for the first time suggested that protons near the neutral plane can change their type of motion, switching to meandering (serpentine) trajectories. Later, Eastwood in [100] conducted numerical modeling using particle tracing in a magnetic field, which allowed estimating the thickness of a relatively thin sheet in the magnetotail during geomagnetic disturbances based on the type of meandering proton trajectories. The first analytic estimates of the TCS thickness were made in [142, 143], where the thickness L_i of a thin ion sheet turned out to be comparable to or even smaller than the proton drift Larmor radius ρ_iD and approximately equal to $L_\mathrm{i} \approx \rho_\mathrm{iD}\varepsilon^{4/3} = \rho_\mathrm{iT}\varepsilon^{1/3}$ (where $\varepsilon = v_\mathrm{T}/v_\mathrm{D}$ is the flux parameter, and $\rho_\mathrm{iT} = \rho_\mathrm{iD}\varepsilon$ is the proton thermal gyroradius; see Section 3.1). This estimate agrees well with observations in the case of strong plasma anisotropy, where $\varepsilon \equiv v_\mathrm{T}/v_\mathrm{D} < 1$. In the limiting case of superstrong flux anisotropy and the condition $v_\mathrm{T}/v_\mathrm{D} < B_z/B_0$ [135, 144], the jumps of the particle invariants turn out to be large ($\Delta I_z \sim I_z$ or even $\Delta I_z > I_z$), and the sheet thickness depends on the ratio of the normal and tangential magnetic components: $L_\mathrm{i} \approx \rho_0(B_z/B_x)^{4/3}$. In the other limiting case $v_\mathrm{T}/v_\mathrm{D} \gg 1$, the thickness of the weakly anisotropic TCS is of the order of the particle thermal gyroradius, $L \sim \rho_\mathrm{T}$ [101].

The new view of particle dynamics was taken into account in the first approaches to construct TCS models, first non-self-consistent [145, 162], and later, self-consistent numerical and analytic TCS models [146, 147], which appeared as models of CS tail compression under the action of a large-scale electric field. Efforts to build a TCS model culminated in the creation of a one-dimensional equilibrium model where electrostatic effects were disregarded (electrons were considered a neutralizing background) [94, 95], while ionic anisotropy of pressures in the TCS and quasiadiabatic dynamics were taken into account. In fact, a new class of one-dimensional TCS models was constructed, where the tension of magnetic field lines in the x direction is balanced by the inertia force of ions crossing the CS plane. The one-dimensionality of the sheet means that it is flat and therefore thin, such that it can be considered a structure lying entirely in the $\{x, y\}$ plane, and all significant characteristics depend only on the z coordinate transverse to the sheet. The entire TCS is supported by interpenetrating fluxes of transient ions with strong longitudinal anisotropy. In the neutral plane, the ions are demagnetized and move along serpentine looping trajectories [35]. In such a sheet, the pressure tensor, which balances the CS and maintains its stationary state, is anisotropic [80, 101, 105, 132].

Historically, a self-consistent model without taking electrostatic effects into account was first proposed in [94, 95] in 2000 and was further developed in 2004, when electrostatic fields required to maintain plasma quasineutrality during the interaction of electron and ion populations were taken into account [78]. It turns out that the spatial structure of the CS in the simplest approximation can be regarded as a practically one-dimensional magnetoplasma structure, whose equilibrium is ensured by the balance between the magnetic tension and the inertia force of ions crossing the CS. The general structure of the TCS is shown schematically in Fig. 7; in Fig. 7a, we can see profiles of the total current density (black solid curve), the electron current density (red curve), and the proton current density (blue dashed line) as functions of the Z coordinate transverse to the sheet. The corresponding profiles of the tangential magnetic field supported by all particles and individual plasma populations are shown in Fig. 7b. Two scales of currents can be clearly distinguished in the figures: a narrow electron current and a wider one, the proton current. This is one of the main characteristics of TCSs, called embedding, when a narrow electron current of magnetized electrons is embedded inside a thicker ion CS supported by demagnetized ions in quasiadiabatic orbits. As a distinctive feature of this type of CS, the dynamics of different plasma populations can differ significantly inside them.

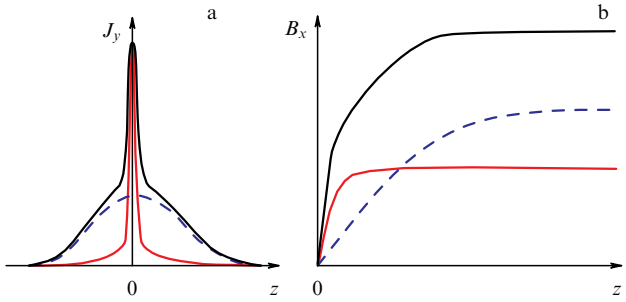

Figure 7. Schematic representation of structure of embedded TCS: (a) profiles of total current density (black line), current density of ions (blue dashed line), and electron density (red line). (b) Profiles of self-consistent tangential magnetic field supported by electrons and ions (shown with respective solid red and dashed blue lines) and total magnetic field (black solid curve). (Adapted from [78].)

Thus, compared to old isotropic models of the magnetotail CS, the TCS model was a new type of plasma equilibrium supported by demagnetized quasiadiabatic protons and magnetized electrons. We show in what follows that equilibrium CSs with anisotropic flows at the sheet edges fundamentally differ in their properties from the equilibria types described in [89, 138, 139, 148].

Let us consider how the main structure of the TCS is formed. It is assumed in the model that the CS thickness (along the Z coordinate) is much smaller than its length along the X and Y coordinates, and hence the CS is practically uniform in the Earth–Sun and morning–evening directions in the mentioned solar-magnetospheric GSM coordinate system (recall that the X-axis is directed from Earth to the Sun, the Z-axis, from south to north along the geomagnetic dipole, and the Y-axis, from east to west). By switching to the de Hoffman–Teller system, the model can be considered quasistationary and the convection electric field E_y, as well as particle acceleration processes associated with the presence of this field, can be ignored.

The value of the ion parameter κ in the tail is sufficiently small for the ion dynamics in the CS to be considered quasiadiabatic [120]. Transient ions are regarded as the main current carriers. The magnetic field has two components, normal and tangential: $\mathbf{B} = \{B_x(z), 0, B_z\}$, where $B_z = \mathrm{const}$. For such a magnetic field configuration, the Vlasov–Maxwell system of equations $\mathrm{rot}\,\mathbf{B} = (4\pi/c)\mathbf{J}$, $\mathrm{d}f/\mathrm{d}t = 0$ reduces to a one-dimensional system of equations

for $B_x(z)$, depending only on the z coordinate,

$$\begin{cases} \dfrac{\mathrm{d}B_x}{\mathrm{d}z} = \dfrac{4\pi}{c}\left\{ e\int v_y f_\mathrm{p}(z,\mathbf{v})\,\mathrm{d}^3\mathbf{v} + j_{\mathrm{e}y}(z)\right\}, \\ B_x(\pm L) = B_{x0}\,, \quad B_y = 0\,, \quad B_z = \mathrm{const}\,, \end{cases} \tag{3}$$

where $f_\mathrm{p}(z,\mathbf{v})$ is the proton distribution function at the CS edges, c is the speed of light, $B_{x0} = |B_x(z)\to\infty|$, and $j_{\mathrm{e}y}$ is the electron drift current.

The quasiadiabaticity condition implies that the following integrals of motion are conserved when a transient particle moves in the TCS magnetic field configuration: total energy $W_0 = mv^2/2 + e\varphi$, generalized momentum $P_y = mv_{y0} - (e/c)A_y(x,z)$, and quasiadiabatic invariant $I_z = \oint p_z\,\mathrm{d}z$, which can be transformed into the form [35, 95]

$$I_z(\mathbf{v},z) = \frac{2m}{\pi}\int_{z_0}^{z_1}\left(v_y^2 + v_z^2 + 2e\{\varphi(z) - \varphi(z')\} - \left\{ v_y + \frac{e}{mc}\int_z^{z'} B_x(z'')\,\mathrm{d}z''\right\}^2\right)^{1/2}\mathrm{d}z'\,, \tag{4}$$

with the integration limits determined from the condition that the expression under the square root in the integrand vanish (or $v_z = 0$).

The ion distribution function, chosen as a shifted Maxwellian distribution outside the CS ($z\to\pm\infty$) [143, 149], has the form

$$f_\mathrm{p}(\mathbf{v}) = \frac{n_0}{(\pi^{1/2}v_\mathrm{T})^3\left(1+\mathrm{erf}\,(v_\mathrm{D}/v_\mathrm{T})\right)} \times \exp\left\{ -\frac{(v_\parallel - v_\mathrm{D})^2 + v_\perp^2}{v_\mathrm{T}^2}\right\}. \tag{5}$$

Here, $v_\parallel$ and $v_\perp$ are the projections of the ion velocity along and across the magnetic field direction, v_D is the average velocity of the plasma flow from the source located at infinity, and v_T is the thermal velocity. To relate the proton distribution function to its asymptotic form outside the sheet, we can use the relation $I_z = (2mc/e)\mu$ between invariant of motion I_z and the magnetic moment $\mu = mv_\perp^2/2B_0$ of the particle [94]. We can then go to the distribution function of passing protons, written in terms of integrals of motion as $f_\mathrm{p}(\mathbf{v})\to f(W_0, I_z)$, i.e.,

$$f(W_0,I_z) = \frac{n_1}{(\pi^{1/2}v_\mathrm{T})^3\left(1+\mathrm{erf}\,(\varepsilon^{-1})\right)} \times \exp\left\{ -\left[\left(\sqrt{\frac{2W_0}{m} - \frac{\omega_0}{m}I_z} - v_\mathrm{D}\right)^2 + \frac{\omega_0}{m}I_z\right] v_\mathrm{T}^{-2}\right\}, \tag{6}$$

where $\omega_0 = eB_0/mc$ is the ion gyrofrequency outside the CS, with $I_z \leqslant mv_0^2/\omega_0$.

This form allows generalizing to the entire CS space. For quasitrapped particles with the invariants of motion $I_z > mv_0^2/\omega_0$, the Maxwell thermal distribution can be rewritten similarly:

$$f_\mathrm{trap} = \frac{n_0}{(\pi^{1/2}v_\mathrm{T})^3\left(1+\mathrm{erf}\,(v_\mathrm{D}/v_\mathrm{T})\right)}\exp\left\{ -\frac{v_\mathrm{D}^2 + (\omega_0/m)I_z}{v_\mathrm{T}^2}\right\}. \tag{7}$$

Both functions match together at the value of the invariant $I_z = mv_0^2/\omega_0$.

3.3 Taking electrostatic effects into account

Let us consider in more detail how electrostatic effects are taken into account in the model of fine equilibrium of anisotropic magnetoplasma [78] and how interaction between electron and ion populations is realized. Because electrons are considered magnetized, they can be treated in the so-called semifluid approximation with an anisotropic pressure tensor (a detailed derivation of the equations can be found in [78] and [35]). It is also assumed that the electron motion along the field lines is fast enough to maintain Boltzmann equilibrium in the presence of an electrostatic potential and the mirror force $-\mu\nabla B$. The quasineutrality condition $n_\mathrm{i}\approx n_\mathrm{e}$ is taken into account, and the nonzero component of the ambipolar electric field $E_z\neq 0$ is also taken into account (it is assumed that $E_y = 0$).

In the semifluid approximation, the electron motion in the direction perpendicular to the magnetic field can be described as a fluid, and, in the parallel direction, in the guiding center approximation,

$$m_\mathrm{e}\frac{\mathrm{d}\mathbf{v}_{\mathrm{e}\perp}}{\mathrm{d}t} = -e\left(\mathbf{E}_\perp + \frac{[\mathbf{v}_\mathrm{e}\times\mathbf{B}]}{c}\right) - \frac{\nabla_\perp p_\mathrm{e}}{n_\mathrm{e}}\,, \tag{8}$$

$$m_\mathrm{e}\frac{\mathrm{d}\mathbf{v}_{\mathrm{e}\parallel}}{\mathrm{d}t} = -e\mathbf{E}_\parallel - \frac{\nabla_\parallel p_\mathrm{e}}{n_\mathrm{e}} - \mu\nabla_\parallel B\,, \tag{9}$$

where $(-e)$ is the electron charge. The last term in (9) is the repulsive diamagnetic force acting on electrons with the magnetic moment μ, $p_\mathrm{e} = p_\perp\delta_{ij} + (p_\parallel - p_\perp)h_ih_j$ is the electron pressure tensor with the unit vector $\mathbf{h} = \mathbf{B}/B$ along the magnetic field direction, and $B = \sqrt{B_x^2 + B_z^2}$ is the total magnetic field. From (9), disregarding the inertia of the fast motion of electrons in the parallel direction and making the substitution $E_\parallel = -\nabla\varphi$, we deduce the equation

$$\nabla\varphi(s) = \frac{1}{en_\mathrm{e}}\nabla_\parallel p_\mathrm{e} + \frac{\mu\nabla_\parallel B(s)}{e}\,, \quad \varphi(\infty)\equiv\varphi_0 = 0\,, \tag{10}$$

where s is a curvilinear coordinate along the field line and the quasineutrality condition $n_\mathrm{e}(\mathbf{r},\varphi(\xi)) = n_\mathrm{i}(\mathbf{r},\varphi(\xi)) = n$ is satisfied. For isothermal electrons, Eqn (10) takes the form of a Boltzmann distribution:

$$\frac{n_\mathrm{e}(s)}{n_0} = \exp\left[\frac{e\left(\varphi(s)-\varphi_0\right) - \mu\left(B(s)-B_0\right)}{T_\mathrm{e}}\right]. \tag{11}$$

To calculate the current density in the direction perpendicular to the magnetic field, we can use the equation for drift electron currents:

$$\mathbf{j}_{\mathrm{e}\perp} = -en_\mathrm{e}c\,\frac{[\mathbf{E}\times\mathbf{h}]}{B} + \frac{c}{B}[\mathbf{h}\times\nabla_\perp p_{\mathrm{e}\perp}] + \frac{c}{B}(p_{\mathrm{e}\parallel} - p_{\mathrm{e}\perp})\left[\mathbf{h}\times(\mathbf{h}\nabla)\mathbf{h}\right], \quad \mathbf{h} = \frac{\mathbf{B}}{B}\,. \tag{12}$$

The first and second terms in (12) describe the drift motion of magnetized electrons under the action of crossed electromagnetic fields and magnetization currents associated with the plasma density gradient across the sheet [35]. The last term in (12) describes the curvature current of electrons in the region of the maximum curvature of the field lines.

Let us introduce normalized variables: z coordinate $Z = z\omega_0/\varepsilon_\mathrm{i}^{4/3}v_\mathrm{D}$, particle velocity $\mathbf{w} = \mathbf{v}/(v_\mathrm{Di}\varepsilon_\mathrm{i}^{2/3})$, magnetic

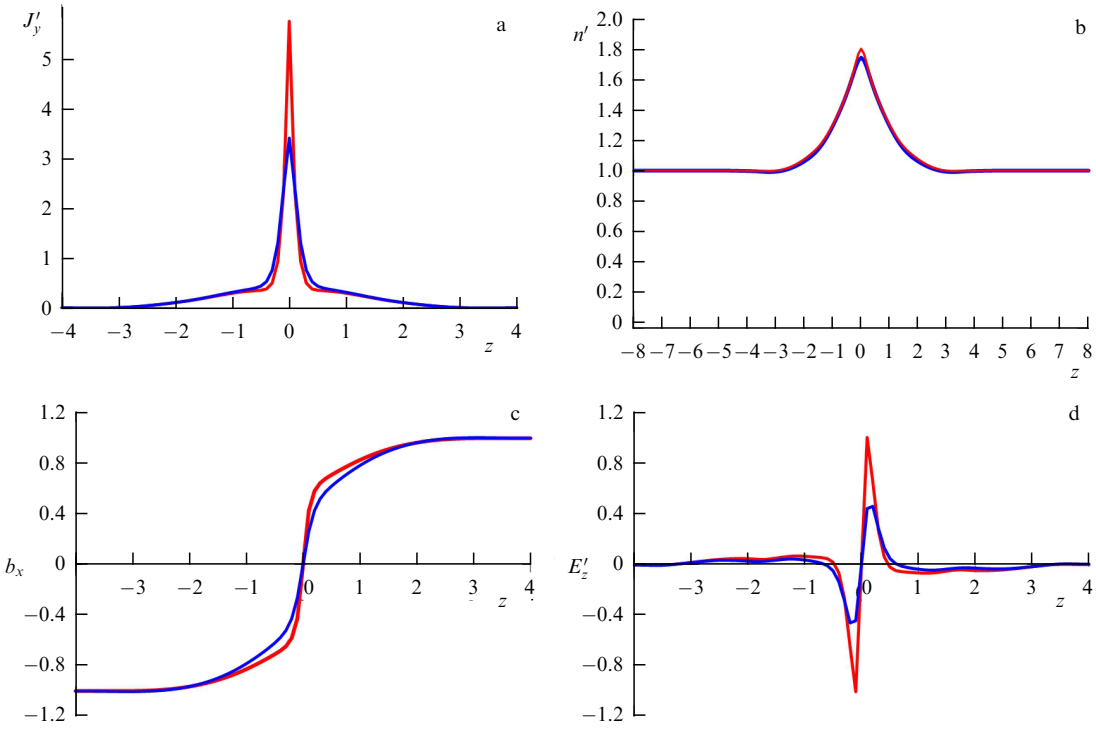

Figure 8. Self-consistent profiles of main normalized characteristics of embedded CS as a function of transverse coordinate z (calculations adapted from [78]), calculated for $\varepsilon_i = 1$ (for all plots): (a) current density $J'_y(z)$, (b) plasma density $n'(z)$, (c) tangential magnetic component $b_x(z)$, and (d) ambipolar electric field $E'_z(z) = -\partial\varphi/\partial z$. Calculations were done with flux anisotropy parameter $\varepsilon_i \equiv v_{Ti}/v_{Di} = 1$ for dimensionless component of normal magnetic field $b_z = B_z/B_0 = 0.05$ (red curves) and $b_z = 0.3$ (blue curves).

field $\mathbf{b} = \mathbf{B}/B_0$ (where $B_0 = B_x(L_i)$ and L_i is the TCS boundary), current density $J'_y(Z) = j_y\varepsilon_i^{-2/3}/(en_0v_{Di})$, plasma density $n' = n/n(L_i)$, and electric field $E'_z = cE_z/(\varepsilon_i^{2/3}B_0v_{Di})$. This allows the TCS to be described using a relatively small set of free parameters, among which the main ones are the flux ion anisotropy $\varepsilon_i = v_{Ti}/v_{Di}$ (where v_{Ti} and v_{Di} are the respective thermal and flux velocities of ions) and the magnitude of the normalized component $b_z = B_z/B_0$ of the normal magnetic field. For normal magnetotail conditions, the ion flux parameter ε_i is less than or of the order of unity, and hence Z is actually normalized to the ion gyroradius at the edges of the ion CS.

The joint solution of the Vlasov–Maxwell system of equations for ions and the simplified MHD equations for electrons, Eqns (4)–(12), allowed obtaining self-consistent solutions of the equilibrium problem, completely consistent with the observational data of the magnetotail CS [77, 78, 80]. Figure 8 shows the calculated self-consistent normalized profiles of the main TCS characteristics as functions of the z coordinate transverse to the sheet. Figure 8a shows the distribution of the current density in the TCS, Fig. 8b, the plasma density, Fig. 8c, the tangential magnetic component of the magnetic field $b_x(z)$, and Fig. 8d, the ambipolar electric field E_z. The calculations were performed for two values of the normal magnetic component of the magnetic field in the TCS, $B_z/B_0 = 0.05$ and 0.3, and are shown by the respective red and blue lines (the calculations are adapted from [78]). A comparison of the profiles in Fig. 8a and b demonstrate the CS embedding inside the plasma sheet: the ion current density profiles at the sheet edges fall to zero, and the plasma density at the sheet edges reaches a constant level. In Figs 8a and c, the electron and ion scales characteristic of the regions of electron and ion dominance can be distinguished clearly. They correspond to different values of the derivatives of the current density and magnetic field in the regions $z \approx 0$ and $z \approx L_i$; therefore, we can say that the narrow electron sheet is embedded inside the thicker ion sheet. It is also evident from Fig. 8a, c that the intensities of the electron and ion currents depend significantly on the normal magnetic component b_z: the larger it is, the smaller the current densities of both embedded sheets supported by quasiadiabatic particles and magnetized electrons become [78, 150]. This is explained by the fact that the particles are increasingly magnetized in the region of a strong magnetic field. Figure 8d shows the distribution of the ambipolar electric field E_z in the TCS, which helps maintain the nested TCS structure as a single whole in the neutral region.

With plasma components such as heavy ions and quasitrapped particles [73, 74, 79] as well as magnetic shear (external or self-consistent [76, 77]) and asymmetric plasma sources [75] in the TCS taken into account, this completely new type of Vlasov equilibrium with multiple nested CSs of different scales could be studied. Due to this property, it [35, 79] was called the Russian-doll model.

A nontrivial problem of obtaining an analytic estimate of the thickness of the embedded electron sheet was associated with embedded models of thin ion-scale sheets. In the hybrid model of embedded TCSs [35, 78], electrons were initially considered a completely magnetized population of particles. This was due to the data from the Cluster satellites available at that time, which, as noted in Section 2.1, mainly allowed distinguishing ion scales, while the embedded electron CSs could be identified by indirect signatures. Although the normal component of the magnetic field B_z in the TCS is

small, estimates of the electron adiabaticity parameter in [55, 56] indicated that, in contrast to the small ion parameter, the electron adiabaticity parameter is $\kappa_e > 1$, and hence the electron dynamics in the TCS is controlled by the magnetic field. Therefore, it could naturally be assumed that the electrons are mostly magnetized and distributed in accordance with the Boltzmann law [78], which means that both the MHD approach and the guiding center approximation can be used to describe their dynamics. However, in these two approaches, it is impossible to estimate the thickness of the embedded electron sheet supported by magnetized particles due to the lack of the analysis of the motion transverse to the magnetic field. For a long time, despite the active development of the hybrid TCS model, scaling of electron sheets was absent. Estimates of the thickness of the electron sheet embedded inside the ion sheet were obtained in [151, 152] two decades later. In these studies, not only was the scale of the electron CSs estimated, but also their close relation to the outer ion sheets was shown.

In [151, 152], a simple analytic TCS model was used, with $\mathbf{B} = B_x(z)\mathbf{e}_x + B_y\mathbf{e}_y + B_z\mathbf{e}_z$. In [151], the shear magnetic component B_y was not taken into account ($B_y = 0$). Later, in [152], its influence was studied, and the anisotropy of the electron component was also taken into account by introducing $\beta_a = 4\pi(p_{e\parallel} - p_{e\perp})/B^2$ as a free parameter (where $B(z) = (B_x^2(z) + B_y^2 + B_z^2)^{1/2}$, and $p_{e\parallel}$ and $p_{e\perp}$ are longitudinal and transverse components of the electron pressure tensor). Recall that configurations with $B_y \neq 0$ are called shear. In them, the planes containing magnetic field lines are tilted to the normal to the neutral plane. The problem was to find a self-consistent profile of the tangential component $B_x(z)$. The input parameters of the model, in addition to the value of the normal component B_z and the electron anisotropy β_a, are the plasma density $n(z)$ and the respective temperatures of electrons and protons, T_e and T_i. These parameters uniquely determined the ion inertial length $\delta_i = c/\omega_{pi}$ (where ω_{pi} is the ion plasma frequency) and the ion Larmor radius ρ_{in} in the neutral sheet field B_z.

Taking into account the magnetic shear, i.e., actually the tilt angle α of magnetic field lines to the normal in the equatorial plane ($\alpha = \arctan(B_y/B_z)$), allowed the frequency of large-scale rotation of protons in the plane $z = 0$ to be estimated as

$$\Omega_{L\min} = \frac{e\sqrt{B_y^2 + B_n^2}}{mc} = \frac{B_n}{B_0}\,\omega_0\,\frac{1}{\cos\alpha}\,, \tag{13}$$

where $\omega_0 = eB_0/mc$, $B_0 \equiv B(L_i)$, and L_i is the ion sheet thickness. Knowing the gyrofrequency at the TCS edges, $\omega_{B\max} = eB(L_i)/mc$, the adiabaticity parameter of protons can be determined as

$$\kappa = \frac{\Omega_{L\min}}{\omega_{B\max}} = \frac{b_n}{\cos\alpha}\sqrt{\frac{L}{\rho_0}}, \quad b_n = \frac{B_n}{B_0}\,. \tag{14}$$

To find the scale of the electron current, the Ampère equation was used:

$$\operatorname{rot}\mathbf{B} = \frac{4\pi}{c}\,(\mathbf{j}_i + \mathbf{j}_e)\,. \tag{15}$$

Here, $\mathbf{j}_i$ is the current density supported by quasiadiabatic ions, and $\mathbf{j}_e$ is the current density supported by electron drifts in the neutral region. Drift electron currents are considered in the guiding center approximation:

$$\mathbf{j}_{e\perp} = \frac{c}{B(z)}\,[\mathbf{h}\times\nabla_\perp p_{e\perp}] + \frac{c}{B(z)}(p_{e\parallel} - p_{e\perp})\big[\mathbf{h}\times(\mathbf{h}\nabla)\mathbf{h}\big]\,, \quad \mathbf{h} = \frac{\mathbf{B}}{|B|}\,. \tag{16}$$

In the magnetic configuration with shear, the estimate of electron current (16) takes the form

$$|\,\mathbf{j}_{e\perp}| \approx c\Delta p_e\,\frac{B_z}{B^4}\,\frac{\partial B_x}{\partial z}\,\frac{B_z}{\cos\alpha}\,, \quad B = \sqrt{B_x^2(z) + B_y^2 + B_z^2}\,. \tag{17}$$

This relation ultimately allowed estimating the y component of the electron current:

$$j_{ey} = \frac{j_{e\perp}}{\cos\alpha} = c\Delta p_e\,\frac{B_z^2}{B^4}\,\frac{\partial B_x}{\partial z}\,\frac{1}{\cos^2\alpha}\,. \tag{18}$$

The anisotropy parameter β_a is included in the hose stability condition in the form

$$p_{e\parallel} - p_{e\perp} = \frac{\beta_a B^2}{4\pi} \tag{19}$$

and lies in the range $0 < \beta_a < 1$, while the hose instability boundary is determined by the condition $\beta_a = 1$. Eventually, Eqn (15) can be simplified and transformed into the form

$$\frac{dB_x}{dz} = \frac{4\pi}{c}\,j_{iy}\left(1 - \frac{\beta_a}{\cos^2\alpha}\,\frac{B_n^2}{B^2}\right)^{-1}. \tag{20}$$

After introducing the dimensionless variables $\tilde{z} = z/\lambda$ (where $\lambda = \delta_i^2/\rho_{in}$, $\delta_i = c/\omega_{pi}$, $\rho_{in} = v_{Ti}/\Omega_{Zi}$, $\Omega_{Zi} = eB_z/m_i c$, $v_{Ti} = \sqrt{2kT_i/m_i}$ is the thermal velocity of an ion, and m_i is its mass) and $b(\tilde{z}) = B_x/B_0 \leqslant 1$, $b_0 = B_0/B_z > 1$, integration of Eqn (20) gives the following estimates for the scaling of the magnetic field in the shear configuration in the region of electron current dominance (at small $\tilde{z}$): $b(\tilde{z}) \sim [3\tilde{z}/(b_0^3\cos^2\alpha)]^{1/3}$ for strong electron anisotropy and $b(\tilde{z}) \sim \tilde{z}/b_0(1-\beta_a)$ for moderate and weak anisotropy of electron pressure. The scale of the ion sheet is determined by the asymptotic value of the magnetic field $B_0 = B_x(z \to L_i)$, where L_i is the ion sheet thickness ($L_i \geqslant \delta_i$).

Thus, final estimates of the electron sheet thicknesses are obtained in two limit cases of electron anisotropy. In the strong anisotropy limit, the electron sheet scaling has the form [152]

$$L_e \sim \frac{\lambda}{3\cos\alpha}\,, \quad \beta_a \geqslant 1\,, \tag{21}$$

and in the case of moderate and weak anisotropy $\beta_a < 1$, we obtain

$$L_e \sim \frac{1-\beta_a}{\cos\alpha}\,\lambda \tag{22}$$

for the electron sheet itself: $L_e \approx \lambda/\cos\alpha$ (where $\lambda = c^2/\omega_{pi}\rho_{in}$ is the ion inertial length, c is the speed of light, ω_{pi} is the ion plasma frequency, $\rho_{in} = v_{Ti}/\Omega_{in}$ is the Larmor radius of proton rotation in the field B_z, v_{Ti} is the thermal ion velocity, and Ω_{in} is the proton rotation frequency in the field B_z) in the case when the characteristic scale of electron motion itself is absent. It can be shown that, at the limit applicability of the description of electrons in the guiding

center approximation ($\kappa_e = 1$), the characteristic thickness of the electron sheet L_e becomes exactly equal to the electron Larmor radius [152].

The analysis performed illustrates complex nonlinear relations between the electron and ion CSs embedded in each other, forming a common current structure.

3.4 Developing the theory. Properties of thin current sheets and kinetic models

Further development of the analytic model in [78, 79, 132, 152] and the transition to its two-dimensional structure were implemented in [88], which allowed estimating the TCS structure over a large length of the tail, depending on the magnitude of the normal magnetic component B_z changing with distance. It turns out that, as the normal component toward Earth increases, the density of the plasma captured by the magnetic field increases, which does not support the current in the tail but leads to the splitting of the current density profiles and the formation of various configurations with two current density maxima and with negative minima on the sides [132]. In this case, the electron current is most deeply inserted inside the CS and creates a narrow peak of the current density in the central part of the sheet. The remaining features of the profiles are due to the dynamics of particles trapped and quasitrapped in the sheet. The TCS model allowed studying and explaining the formation mechanisms of three types of CSs (with one, two, and three maxima) and the asymmetric structures [24, 35, 72], i.e., all the main features of the observed TCSs listed in Section 2.1.

It can be added that the development of the kinetic approach to modeling thin sheets has allowed not only explaining the main features of their configurations observed *in situ* [35, 61, 91, 92] but also predicting new properties of their structure and dynamics that could not be explained based on observational data alone.

(1) The TCS has the ion thickness (from hundreds to several thousand kilometers for 10-keV magnetotail protons), but, in its very center, there can be a embedded electron sheet an order of magnitude thinner, with a thickness of several ten kilometers (the electron energies in the tail are significantly lower than the proton energies). The current in the TCS is maintained by plasma flows into the sheet; the sheet as a whole is nested inside a much wider plasma layer.

(2) The dynamics of protons in the TCS is quasiadiabatic, as shown in [120]. Quasiadiabatic dynamics determines the internal structure of the CS. This implies demagnetization of ions upon entering the CS and their serpentine motion along a semicircle in the neutral plane, which the particle alternately crosses, moving between the northern and southern hemispheres (such a trajectory is also called meandering).

(3) Because the gyroradii of electrons are significantly smaller than the proton sheet thickness, it was concluded that electrons are completely magnetized inside the CS [78, 151, 152]. This indicated the need to take the ambipolar electric field E_z into account, which arises due to the different dynamics of plasma particles. Due to the presence of the ambipolar field, the electron population depended quite strongly on the properties of the proton population, for example, on the thickness of the surrounding ion CS.

(4) Ions are the main current-carrying particles and, as estimated in [79], support more than 70% of the total current (heavy oxygen ions can join the proton population in the magnetotail). The current density profile created by demagnetized quasiadiabatic ions is determined by their dynamics (meandering motion in the neutral region) and, in general, the ratio between the populations of transient and quasitrapped particles. Taking them into account allows predicting the formation of multipeak current density profiles [35].

(5) The asymmetry of the CS can be determined, in particular, by the following factors: the asymmetry of plasma sources [75], the influence of the shear magnetic component present in the TCS, and, possibly, the seasonal change in the tilt of Earth's magnetic dipole [76, 77].

(6) The integral electron current, whose amplitude can under certain conditions be much greater than that of the proton current, is no more than 30% of the total current in the system [79]. The electron current supported by the curvature currents of electrons is very narrow, its magnitude being inversely proportional to the curvature radius of the magnetic field lines in the vicinity of the neutral plane $z = 0$. At a small thickness, even a strong electron current can make a small contribution to the total current.

(7) The TCS is characterized by a embedded structure, with a narrow electron current embedded inside a wider proton current, and the entire CS as a whole embedded inside a much wider plasma sheet. The embedding property is an important and distinctive property of CSs. Due to it, an ambipolar electric field maintained in the system supports the TCS as a whole, while the condition of hose stability of the sheet is satisfied [149].

(8) The TCS is metastable, meaning that it is stable at the beginning of substorm development, but can spontaneously be destroyed under the influence of the emerging tearing instability [98], giving rise to various substorm disturbances in the magnetosphere.

'As knowledge about the formation and dynamical properties of TCSs was being developed based on observations in the magnetosphere, a hotly debated question, rooted in principles, arose about their role in the development of magnetospheric disturbances [35, 45, 135]. As modern observations and modeling results show, just the TCSs are the key structures that shape the geomagnetic response to the interaction of the magnetosphere with the SW. The main scenario for the formation of TCSs in the magnetosphere during fairly frequent magnetic substorms is as follows: the heliospheric CS is strongly folded [153, 154]. In the areas (sectors) between its folds, the interplanetary magnetic field (IMF) can have a pronounced northern or southern direction. Earth, moving in the plane of the ecliptic, periodically crosses the boundaries between the folds (sectors), and the direction of the IMF reverses. Magnetic substorms always begin with the arrival of the southern IMF, which on the daytime magnetopause reconnects with the oppositely directed geomagnetic field, and then the reconnected magnetic flux is transferred to the tail. Under the influence of the growing magnetic field, over a period from 0.5 to 2 hours, the magnetotail CS thins from the initial thickness of several R_E to several hundred or thousand kilometers. A TCS extended along the tail forms [35] and accumulates excess free energy [45, 135]. In the process of evolution, tearing instability can develop in the TCS, such that the flat current disintegrates into one or several current ropes (so-called plasmoids). Drift motion of plasmoids detached from the geomagnetic field contribute to their movement into the tail and then beyond the magnetosphere. At the same time, waves of magnetic field dipolarization moving toward Earth arise [155, 156], restoring the original shape of the magnetosphere. Streams of particles accelerated by reconnection are released into the

atmosphere in the region of the auroral oval [157, 158]. The substorm ceases when the main part of the energy that entered Earth's magnetic field from the outside dissipates from the magnetosphere together with plasmoids and accelerated plasma streams. The energy transformation cycle is completed by restoring the magnetosphere to its original state [159], to be repeated the next time the excess energy from the SW is introduced into it.

3.5 Ion tearing instability as a mechanism of energy release and magnetic reconnection in metastable thin current sheets

The study of the stability of the quasiadiabatic model of a multiscale embedded TCS actually put an end to the preceding scientific discussions about the absolute stability of the magnetotail CS [45, 92, 98]. The stability under the ion tearing mode was estimated in the framework of linear stability theory. The energy principle was used, according to which the energy balance in a perturbed system during the development of the tearing mode can be represented as [92, 98]

$$\delta W = W_{\rm b} + W_{\rm free} - W_{\rm e}\,. \tag{23}$$

The first term on the right-hand side of (23) reflects the energy expenditure on the creation of the perturbed magnetic field leading to reconnection, the second is the free energy of the sheet providing the attraction of parallel current filaments to each other, and the third is the energy expenditure on the compression/rarefaction of the electron component of the plasma (the effect of electron compressibility) in the presence of the normal component B_z. The term $W_{\rm free}$ actually determines the free energy stored in the TCS, which provides the development of the tearing disturbance. Estimates give $W_{\rm free} < 0$, while the other two terms must be positive: $W_{\rm b}, W_{\rm e} > 0$. A detailed derivation and description of the energy functional can be found in [45, 92, 98].

The energy functional δW reflects the energy difference between the disturbed and undisturbed states of the CS. If $\delta W < 0$, then the energy of the disturbed state is lower than in the undisturbed state, and hence the transition to a lower-energy level is advantageous for the system, and the development of the tearing mode is possible; otherwise, if $\delta W > 0$, the sheet is completely stable. It was shown in [98] that the free energy in the TCS is several times higher than that of the Harris CS, and hence the development of the tearing mode is possible for certain parameters of the system. CSs with a small normal magnetic component $B_z \sim \{0.1\text{–}0.2\}B_{x0}$ (where B_{x0} is the tangential field at the TCS edges) turn out to be unstable, which accords with the observed values in the magnetospheric tail [92].

The study of stability for different parameters demonstrated the key role of embedded CSs in the development of magnetic disturbances. In [98], a study of a hybrid TCS model for stability with respect to the tearing mode revealed a bounded region in the phase space of the system where the TCS is unstable. Outside this region is the region of complete stability. Later, the CS metastability mechanism in the tail of Earth's magnetosphere was studied in detail in [160]. It was shown that, if the CS characteristics during the thinning of the tail CS in a magnetospheric substorm are represented by points in the parametric space, then these points move in the parameter region toward the instability region. Arriving at the instability region predicted in the framework of the model developed above, the CSs are destroyed [160].

The simulation results also show that the development of the ion tearing mode significantly depends on the electron temperature $T_{\rm e}$ (it increases with increasing $T_{\rm e}$) and on the thickness of the outer ion sheet (the thinner it is, the stronger the instability). In general, it was shown that, in the TCS, which has a well-defined nested structure, the development of instability is provided by the development of the ion tearing mode, while the characteristics of the narrower electron current can indirectly affect the spatiotemporal dynamics of the sheet disruption and the onset of reconnection in it [45].

4. Inside the singularity: electron scale and superthin sheets

4.1 High-resolution observations: superthin electron sheets in space. MMS mission

As noted in Section 3, multisatellite studies of magnetoplasma structures by the Cluster and THEMIS missions stimulated the next step in the development of satellite observations: the launch of the MMS mission, which repeated the Cluster concept in terms of the tetrahedral four-satellite configuration, but with inter-satellite distances tens and hundreds of times smaller [161]. For example, in the geomagnetic tail CS, the distance between the satellites of the MMS tetrahedron near the orbital apogee is ~ 20 km, which is approximately equal to several electron gyroradii ($\rho_{\rm e}$). The Cluster mission was actually devoted to the study of the ion kinetics in TCSs at the magnetoplasma boundaries and in magnetic reconnection, but the MMS mission was tasked with studying the role of electron physics in the formation and dynamics of these structures.

Due to the high temporal resolution of magnetic field measurements and 3D electron velocity distribution functions in the tail of Earth's magnetosphere and in the magnetopause CS, in the magnetosheath, and at the front of the bow shock, it was for the first time possible to observe intense superthin CSs with a thickness of the order of several $\rho_{\rm e}$ and with a current density tens and sometimes hundreds of times greater than the current density in the ion TCS [162–166]. It has been shown that intense STCSs are generated mainly by electrons, whose flow velocity is at least several times higher than the corresponding flow velocity of ions.

Figure 9 shows an example of STCS observations by the MMS satellites on July 6, 2017 during the propagation of a fast plasma stream (FPS) moving away from Earth at a speed reaching 1000 km s^{-1} [167]. An FPS directed away from Earth indicates the presence of an active X-line between the MMS satellites and Earth [49]. At the time of the STCS observation, the MMS satellite quartet had the coordinates $[-24, 0.5, 4.7]R_{\rm E}$ in the GSE coordinate system and was located near the neutral plane of the plasma layer (PL) of the geomagnetic tail. The current density in the STCS, measured as $\mathrm{rot}\,\mathbf{B}$ from four-point magnetic field measurements, was $J_B \sim 80$ nA m^{-2}. The STCS thickness was $L \sim 45$ km $\sim 4\rho_{\rm e}$. To analyze the STCS structure, it is more convenient to use the local LMN coordinate system: its **N**-axis is oriented along the direction of the minimum variation of the magnetic field through the sheet, determined by the minimum variance analysis method [168]; the **L**-axis coincides with the direction of the maximum variation, and the **M**-axis complements the right triple of orthogonal

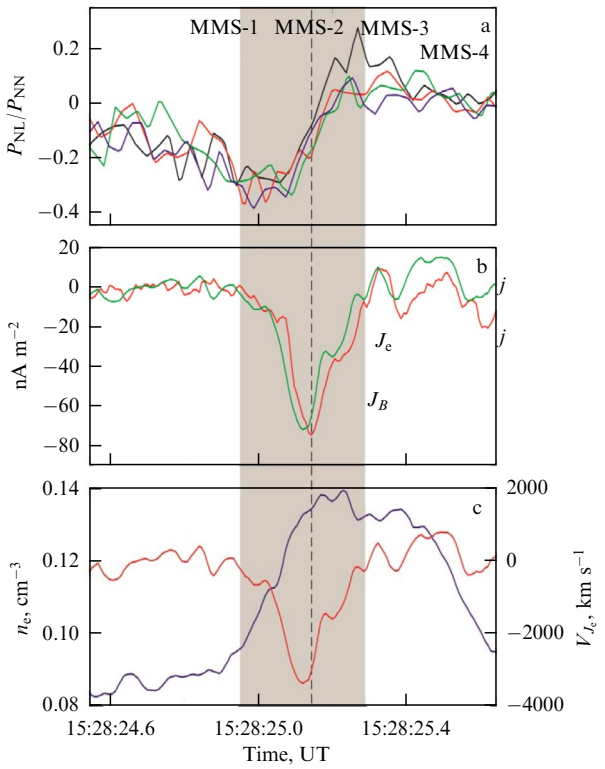

Figure 9. STCS observation by MMS satellites on 6.07.2017. From top down: (a) time profile of spatial variation of off-diagonal component of pressure tensor P_{NL} of current-carrying electron population, normalized to diagonal component P_{NN}, observed by four MMS satellites; (b) time profile of current density J_B (red line) and electron current density J_e calculated in barycenter of MMS satellite quartet (green line); (c) time profiles of density (blue line) and flux velocity of current-carrying electrons along current direction in sheet (red line). STCS observation interval is shown with shades of gray. (Adapted from [167].)

vectors. In the case of a 1D CS, the **M**-axis coincides with the direction of the current in the sheet. It can be seen from Fig. 9b that the time profile of the current density J_B (shown with the red line) almost exactly coincides with the time profile of the current density J_e created by electrons with energies greater than 1.2 keV (shown with the green line) in the barycenter of the MMS quartet. This means that the current in the STCS is generated almost entirely by the superthermal electron population.

The current-carrying electron population is demagnetized, as evidenced by the presence of a significant bipolar variation in the off-diagonal component of the pressure tensor P_{NL} observed by all four MMS satellites when crossing the STCS (Fig. 9a). The intense current in the STCS is then almost entirely provided by the gradient of this off-diagonal component of the pressure tensor of the current-carrying electron population along the normal to the STCS [167]. Thus, the formation of an STCS with a sheet thickness of the order of or less than several gyroradii of thermal electrons occurs similarly to the formation of ion TCSs with a thickness of the order of a proton gyroradius [101]. Namely, the intense current in the STCS is created by the demagnetized population of electrons in the Speiser orbits [99], and the tension balance in the sheet is maintained by the gradient of the off-diagonal terms of the pressure tensor of the current-carrying electron population.

Importantly, the time profile of the component of the current-carrying electron population flow velocity along the direction of the current in the STCS, V_J, almost completely coincides with the current density profile in the sheet, J_B, while the time profile of the current-carrying electron density does not coincide with the profile of J_B (Fig. 9c). This indicates that the intense current in the STCS is provided by the high flow velocity of the current-carrying electron population, and not by an increase in its density in the center of the sheet, as was assumed in the Harris CS model.

This feature of electron STCSs was later confirmed by statistical studies. In [169], MMS observations in the PL of the tail were analyzed as regards the propagation of 41 FPSs directed toward Earth and 37 FPSs moving away from Earth. During the FPS intervals, many (more than 1000) intense STCSs with a current density $J_B \geqslant 30$ nA m^{-2} were observed in the PL, which is several times greater than the current density in the unperturbed CS of the tail. In all cases, the leading contribution to the current was made by the electron population. The variation in the electron flow velocity along the current direction in the STCS, normalized to the maximum value of the modulus of this component in a given STCS, $\Delta V_J/|V_J|_{max}$, was much greater than the corresponding variation in the electron density normalized to the maximum electron density in a given STCS: $\Delta n_e/(n_e)_{max}$ (Fig. 10a, b). Therefore, the current in the STCS is caused by a significant increase in the electron flow velocity, rather than by an increase in their concentration. This property was previously deduced from a simulation of intense current structures generated in cold turbulent plasma [170]. It was shown in the simulation that intense current structures are mainly longitudinal and the high current density in them is caused by a significant increase in the electron flow velocity, which makes it much greater than the ion flow velocity, $V_e/V_i \gg 1$. In this case, the change in concentration on the scale of the sheet did not exceed 10%. In a hot plasma, the STCSs in PLs are almost always produced by high-speed super-Alfvén electron beams whose velocity along the current direction is several or sometimes tens of times greater than the absolute value of the corresponding component of the ion flow velocity.

Regardless of the direction of the FPS, STCSs were observed at arbitrary distances from the neutral plane of the PL, which indicates that these current structures are not necessarily part of the transverse CS tail, but can represent independent structures self-organizing in the turbulent plasma of the PL, disturbed by the propagation of the FPS. Indeed, in the absence of an FPS, intense STCSs are hardly observed in the PL. Only one case of observing an intense STCS in the absence of the FPS is known in the literature [162].

In most intense STCSs observed in a PL, the electric current is directed along the external magnetic field. Such STCSs are generated by accelerated electron beams of superthermal energies moving along the magnetic field lines. It was previously reported that STCSs created by longitudinal electron beams are observed only in the boundary plasma layer [72, 162]; however, as our statistical studies show, such STCSs can also be observed near the neutral plane. Topologically, this means that the PL contains secondary sources of electron beam acceleration generating such STCSs, which can be located at some, possibly significant, radial distance from the primary X-line generating the large-scale FPS. This scenario is illustrated in Fig. 11.

A number of studies reported the observation of a high power density of energy conversion not in the primary X-line

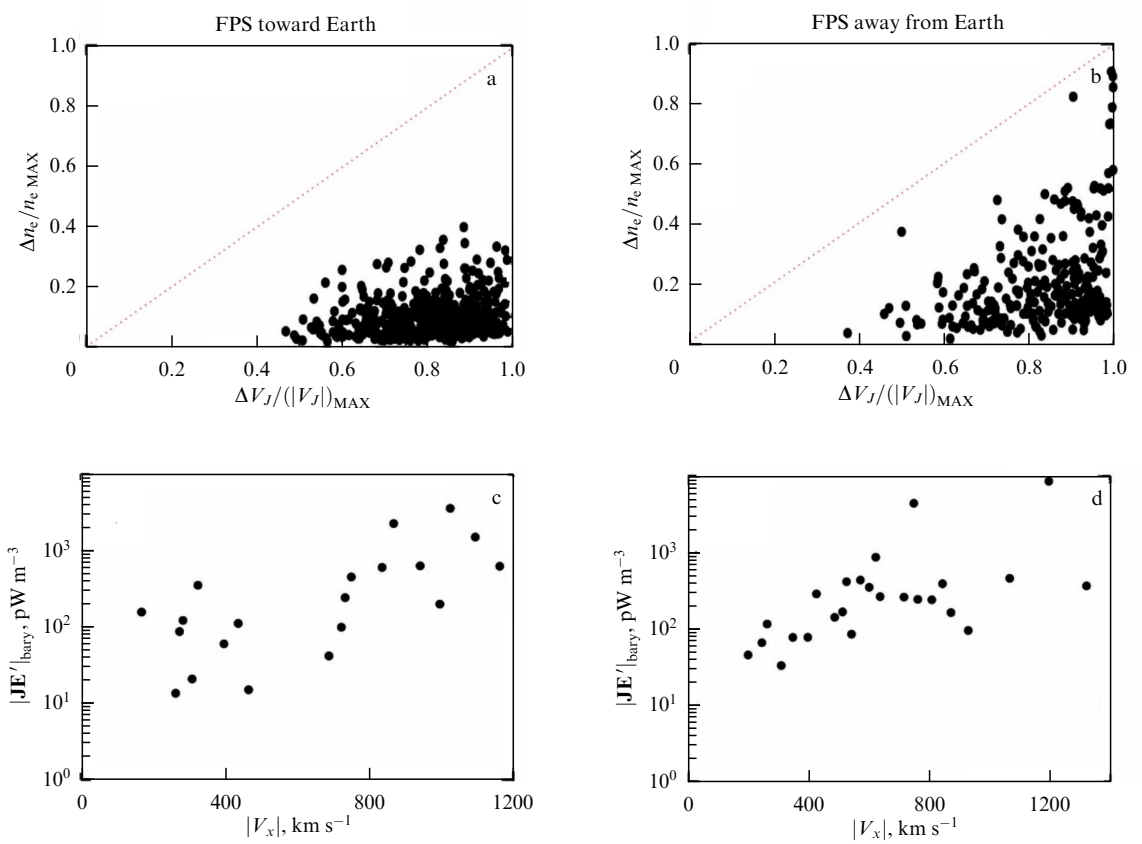

Figure 10. Relative variations in characteristics of electron fluxes: electron densities as function of flux velocity modulus along current direction, observed in each STCS from database published in [169] for FPS intervals directed (a) toward Earth and (b) away from Earth; dependences of maximum modulus of **JE**′ parameter, observed in each FPS interval, on velocity modulus of a given FPS for fluxes directed (c) toward Earth and (d) away from Earth. (Adapted from [169].)

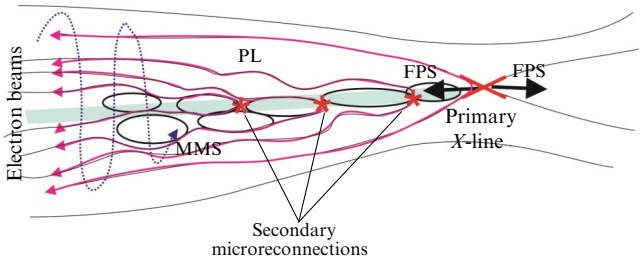

Figure 11. Illustration of scenario of generation of multiple accelerated longitudinal electron beams (shown by crimson arrows) generating a longitudinal STCS in PL of geomagnetic tail during propagation of FPS (shown by black arrows) from primary *X*-line. Electron beams are accelerated in secondary sources (shown by red asterisks), possibly microreconnections formed at boundaries of magnetic islands carried by FPS from primary *X*-line. Transverse CS of tail is shown in blue shading. Trajectory of MMS satellites in plasma rest frame is shown by blue dotted line. Magnetic field lines are shown by black lines. (Adapted from [169].)

but at some distance from it, in *O*-line magnetic structures [166, 171, 172]. Secondary sources of electron acceleration can be secondary microreconnections or, as they are also called in the literature, electron reconnections. Secondary microreconnections received this name because these processes occur without the observed participation of ions [173–177].

Indeed, many STCSs exhibit characteristics typical of classical diffusion regions required for reconnection (see, e.g., [26, 178]): violation of the frozen-in electron population associated with strong nonideal electric fields $\mathbf{E}'$ that can reach tens of mV m^{-1}; a high electric current density J concentrated in a thin sheet of thickness $\sim d_e$ (where d_e is the electron inertial length); and a high power density of the released energy **JE**′, reaching hundreds and sometimes several thousand pW m^{-3} [179]. However, the question of the further development of electron reconnection remains open. In a number of studies, it was assumed that secondary electron reconnection is the initial (or transient) stage of development of a new *X*-line on the ion kinetic scale [180]. In modeling, such a process was successfully reproduced when a strong external driver was applied to the secondary electron diffusion region associated with STCSs in the form of an increase in the magnetic flux in the tail lobes or strong fluctuations in the flow velocity of the FPS accelerated in the primary *X*-line [181–183]. However, direct satellite observations of such a process have not yet been made.

In this regard, the question of the mechanisms of formation and evolution of STCSs remains open. It is only known that most intense STCSs are formed by electron longitudinal beams, and less often, by electron flows moving perpendicular to the external magnetic field; the current-carrying electron population is superthermal and super-Alfvén and has a velocity significantly exceeding the ion flow velocity. According to our statistical studies, the duration of an STCS observation is no more than 1 s, i.e., satellites observe STCSs at some phase of their evolution, and it is practically impossible to trace the further development of the sheet. Theory shows that fast electron tearing instability

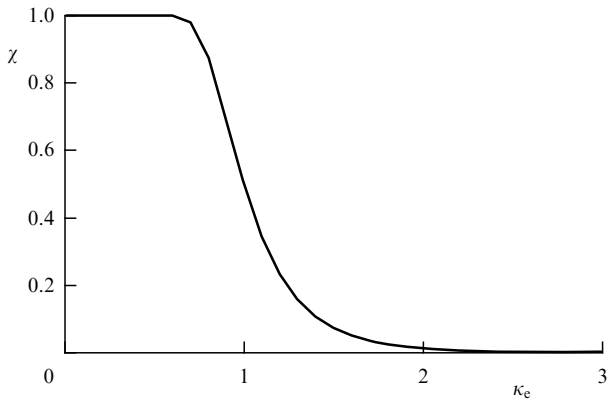

Figure 12. Dependence of fraction of demagnetized electrons χ on adiabaticity parameter κ_e.

can develop in such superthin sheets [184]. Observations of bursts of strong electric fields, in some cases reaching tens of mV m^{-1} inside and at the edges of STCSs, also indicate their possible nonstationarity. It can be assumed that the external driver, which is most likely the FPS and the associated enhancement of the convection electric field $\mathbf{E}_C = -\mathbf{V}_i \times \mathbf{B}$ (where $\mathbf{V}_i$ is the ion flow velocity), causes the development of fast electromagnetic fluctuations in the PL, which, in turn, contribute to the acceleration of the electron beams forming the STCS. Electron beams can also be accelerated in nonstationary magnetic structures frozen into the FPS, such as magnetic islands and dipolarization and antidipolarization fronts, and as a result of secondary microreconnections associated with these magnetic structures. The further evolution and subsequent decay of an STCS again cause the generation of induced electric fields that accelerate a new electron beam, which forms a new STCS in another region in the PL. This process has a cascade nature and generally explains the formation of multiple intense STCSs with different spatial orientations observed in the PL at arbitrary distances from the neutral plane during the propagation of the FPS [169].

4.2 Multiscale model of superthin electron sheet with magnetized and demagnetized particles

Research into CSs in Earth's magnetosphere has long been based on the assumption that electrons remain magnetized and their contribution to the current is due to pressure anisotropy. However, with the advent of high-precision data from the MMS mission, it became clear that the anisotropy of the electron pressure in the observed STCSs is small, while the pressure tensor is nongyrotropic, indicating a significantly nonadiabatic motion of electrons [167, 185]. This discovery required the development of a new combined model where the electron dynamics is divided into two components: magnetized (described in the guiding center approximation) and demagnetized (described in the quasiadiabatic approximation, similarly to ions) [186]. The development of such a model became possible due to the existing detailed theory of nonadiabatic particle motion, which takes approximate invariants other than the magnetic moment into account [35, 120].

The key parameter of the model was the weighing coefficient $\chi = n^{De}(\infty)/n_0$, which characterizes the fraction of demagnetized electrons (De) in the total population. This quantity depends on the adiabaticity parameter $\kappa_e \approx B_n/B_0\sqrt{L/\rho_e}$ [120]. It is assumed that χ decreases monotonically with increasing κ_e: from $\chi \approx 1$ at $\kappa_e \leqslant 0.5$ (fully demagnetized electrons) to $\chi \approx 0$ at $\kappa_e \geqslant 2$ (fully magnetized electrons), taking an intermediate value $\chi = 0.5$ at $\kappa_e = 1$, as shown in Fig. 12. It should be recognized that particles near the narrow region $\kappa_e = 1$ exhibit strong chaotic motion [120, 187], which is not fully covered by our models ($\mu_e \approx$ const or $I_z^{(e)} \approx$ const). However, as calculations show [120, 188], the contribution of chaotic particles to the currents is negligibly small, which justifies the approximation used in the model.

The main result of the new one-dimensional self-consistent model [186] was proof that the presence of demagnetized electrons enhances the peak current density in the neutral plane by 3 to 5 times and reduces the effective sheet thickness to several electron gyroradii ($L_e \sim (2\text{–}5)\rho_e$). As a typical example, we consider a configuration with a 50% demagnetized electron population at $B_n/B_0 = 0.1$. Analysis of the CS profiles in Fig. 13 for demagnetized protons (Di) and electrons (De) with the velocity anisotropy $\varepsilon_{Di,e}^{-1} = v_{Di,e}/v_{Ti,e} = 1$ and for magnetized electrons (Me) with the weak pressure anisotropy $\Lambda_{Me} = \mu_0(p_{\|e} - p_{\perp e})/B^2 = 0.1$ suggests the following conclusions:

(1) Plasma density: demagnetized electrons (De) demonstrate rarefaction of their density near the neutral plane with a sharp compaction in the center and contribute to the

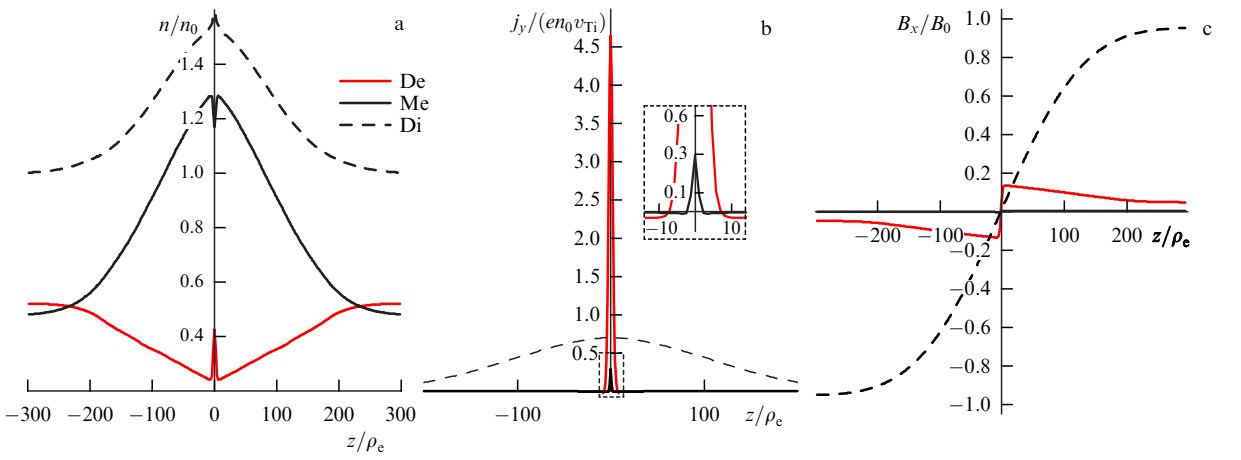

Figure 13. Profiles of dimensionless STCS characteristics with half-demagnetized electron population ($\chi = 0.5$): (a) partial concentrations of demagnetized protons (Di) and magnetized + demagnetized electrons (Me + De); (b) their partial current densities and (c) corresponding B_x components of magnetic fields.

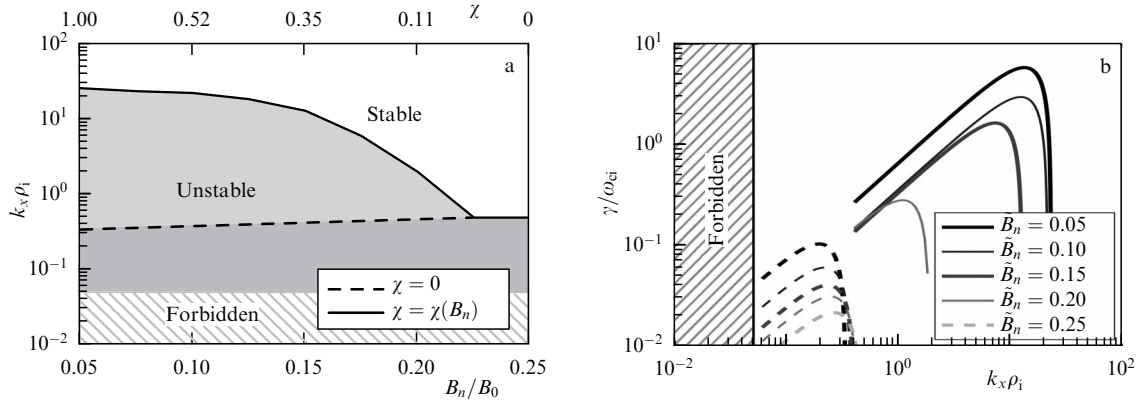

Figure 14. Comparative characteristics of tearing modes. (a) Marginal wave numbers $k_x\rho_i$ as functions of ratio B_n/B_0. (b) Growth rates γ/ω_{ci} depending on $k_x\rho_i$. Parameters are $\varepsilon_{Di,e} = 1$ and $\Lambda_{Me} = 0.1$. Solid lines correspond to STCS with demagnetized electrons ($\chi = \chi(B_n)$; see Fig. 12), and dashed lines, without them ($\chi = 0$).

compression of the total plasma density (Di). Magnetized electrons (Me) maintain plasma quasineutrality ($n^{Di} = n^{De} + n^{Me}$).

(2) Current density: the current of demagnetized electrons dominates ($\sim 80\%$), forming a superthin sheet ($L_e \sim 5\rho_e$) embedded in the ion CS. The contribution of magnetized electrons is insignificant ($\sim 5\%$).

(3) Magnetic field: the intense electron current creates extreme magnetic field gradients ($\nabla B \sim B_0/\rho_e$) at the CS center, determining the steepness of the $B_x(z)$ profile, while the ions form a large-scale structure. The relative contribution of electrons is $B^{De+Me}(\infty)/B_0 \approx 6\%$.

These results are in good agreement with MMS observations, where currents of $\sim$ 50–100 nA m^{-2} were recorded at thicknesses of $\sim$ 20–50 km ($\sim (1–5)\rho_e$) even in the presence of weak electron anisotropy ($p_{\|e} \approx p_{\perp e}$).

4.3 Electron tearing mode. Role of multiscale and embedding in development of cascade reconnection processes in cosmic plasma. Contribution of proton and electron populations to processes of magnetic island fragmentation and energy dissipation

Observations of STCSs have revived interest in the classic problem of their stability. While previous studies have mainly focused on the stability of TCSs and the development of ion tearing modes in them, the presence of partially demagnetized electrons in STCSs opens up new possibilities for studying electron tearing modes, characterized by significantly smaller time and space scales than ionic modes have [184].

Figure 14 demonstrates the difference in the behavior of marginal wave numbers and tearing mode growth rates depending on the presence of demagnetized electrons (De) in the sheet. As the B_n/B_0 ratio decreases, the fraction of demagnetized electrons χ increases, which leads to two important effects:

- thinning of the STCS and accumulation of free energy $W_{free} \sim L^{-2}$;
- reduction in the stabilizing contribution of magnetized electrons ($W_e \sim n^{Me}/B_n^2$).

These factors contribute to the development of a fast electron tearing mode at short wavelengths. It is noteworthy that the instability increments in STCSs with demagnetized electrons are two orders of magnitude higher than in sheets without such a population (Fig. 14b). The time scales of such processes amount to seconds, while the characteristic times of ion instabilities development are minutes or even tens of minutes, which is comparable to the duration of large-scale substorms.

Figure 14a shows that the STCS instability region shifts toward larger wave numbers (short wavelengths). This indicates the formation of increasingly small-scale, rapidly evolving structures (magnetic islands), which fundamentally changes the traditional ideas about the CS dynamics. Such observations became possible due to modern high-precision MMS measurements, which act as a kind of magnifying glass for studying microphysical processes in plasma.

In what follows, we consider an example of an observation by MMS satellites of the evolution of an STCS associated with the development of the electron tearing mode (Fig. 16a). This STCS was observed on July 6, 2017 at 16:01:21–16:01:32 UT near the neutral plane of the PL tail inside the magnetic island transferred to the observation point by an FPS moving toward Earth from the active primary X-line [167]. Figure 15 shows the time profiles of three components of the magnetic field (Fig. 15a), the current density calculated from magnetic measurements (Fig. 15b), and the flow velocity of ions and electrons (Fig. 15c and d, respectively).

During this interval, several bursts with amplitudes > 30 nA m^{-2} are observed in the current density, associated with the intersections of intense STCSs by the MMS satellites. To discuss the STCS evolution, we consider two bursts observed at times III and IV (marked with vertical dashed lines in Fig. 15) and also analyze the prehistory of plasma processes observed at times before the onset of the STCS evolution (times I and II) and in the post-tearing period (time V).

The left-hand side of Fig. 16b schematically shows the evolution of a magnetic island and the intense STCS associated with it. This magnetic island was one of the many magnetic islands transported by the FPS from the primary X-line to the observation point [167]. Its uniqueness lay in the fact that the MMS satellites, while inside the island, remained near the neutral plane of the PL for almost 10 s. This allowed tracing the evolution of the electron velocity distribution function in the STCS and the change in the thickness and density of the current in the STCS [184].

At time I, the MMS quartet was in the southern part of the PL outside the neutral plane, on the boundary of a large-scale

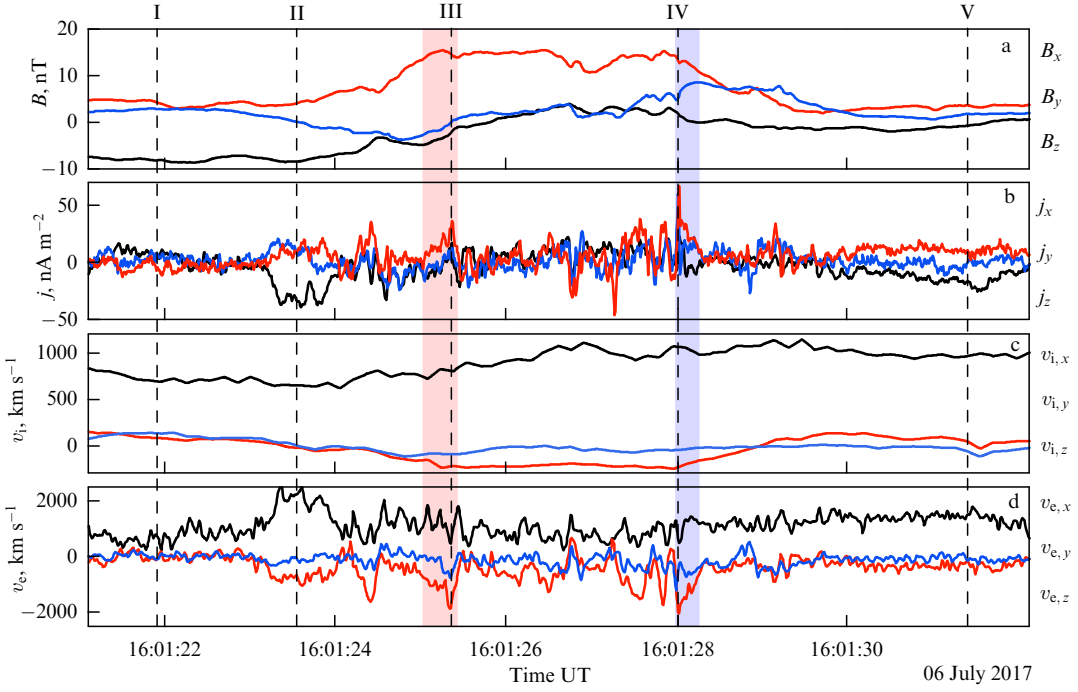

Figure 15. Example of STCS evolution observed by MMS-1 satellite near neutral plane of PL, which resulted in development of electron tearing mode. From top down: time profile of (a) three components of magnetic field, (b) current density, (c) flow velocity of ions and (d) electrons. (Adapted from [184].)

magnetic island, as evidenced by the observation of two counter electron beams moving along the magnetic field lines with nearly identical velocities and intensities (see the electron distribution functions corresponding to time I on the right side of Fig. 16b). After ~ 2 s, at time II, the MMS satellites suddenly started observing a strongly accelerated electron beam moving toward Earth with a parallel velocity significantly exceeding that of the corresponding counter-directed beam (see the distribution functions at time II in Fig. 16b), but no changes occurred in the flow velocity of the ion FPS (Fig. 15c). This indicates the formation of an additional source of electron acceleration at a somewhat longer distance from Earth than the position of MMS satellites. It can be assumed that such an additional source of electron beam acceleration was secondary electron reconnection, which could occur as a result of the development of the electron tearing mode. This could in turn lead to the fragmentation of a large-scale island into smaller ones (see the illustration for instant II in the left part of Fig. 16b). The accelerated electron beam generated an STCS with a strong current $J_x \sim -40$ nA m^{-2} (Fig. 15b, d).

Next, the MMS quartet moved toward the neutral plane and entered a smaller-scale magnetic island, presumably formed as a result of fragmentation of the initial large-scale island (instant III). The presence of such an island is indicated by the observation of a negative variation in the B_z field, marking the leading edge of the island moving toward Earth (Fig. 15a). Near the neutral plane, the MMS observed an STCS with the current directed along the magnetic field due to the presence of the shear magnetic field component. This current, with a density exceeding 30 nA m^{-2} (Fig. 15b), was generated by a longitudinal electron beam that moved antiparallel to the magnetic field without a counter-directed beam (see the distribution function for instant III in Fig. 16b). Approximately at instant III, the electron tearing mode began to develop. By instant IV, which is only 2.7 s away from instant III, there was a rapid thinning and increase in the current density in the STCS by a factor of 1.8 compared to the current density observed at instant III (Fig. 15b). An intensification of the current-carrying electron beam was simultaneously observed in the electron velocity distribution function (see Fig. 16).

The STCS thinning led to a rapid increase in the relative concentration of demagnetized electrons in the sheet. In the STCS observed at instant III, the electron population with energies > 700 eV was demagnetized ($\kappa_e < 1$). This demagnetized population constituted about 30% of the total electron concentration in the STCS. However, after the STCS thinning at instant IV, the low-energy boundary of the demagnetized electron population decreased to ~ 200 eV, resulting in a sharp increase in the fraction of demagnetized electrons in the sheet (to $\sim 80\%$). Simultaneously, the fraction of Speiser [99] electrons, which make the main contribution to the current, increased to $\sim 45\%$ of the entire electron population. In the electron distribution functions observed at instants III and IV, the low-energy boundary of the demagnetized population is shown by a black circle. Thus, by instant IV, the concentration of demagnetized electrons increased, and the stabilizing effect of magnetized electrons decreased due to a decrease in their concentration. Such an STCS becomes unstable under the excitation of the electron tearing mode, whose development leads to the fragmentation of the magnetic island containing the STCS into smaller islands. The observation of a positive variation in the B_z field indicates the intersection of the rear boundary of the small-scale island (Fig. 15a). Assuming an exponential instability growth ($j \sim \exp(t/T)$) and taking the current density gain $\Gamma = 1.8$ into account, the instability development time can be estimated as $T \sim \Delta t/\ln\Gamma \sim 4.5$ s. The radial size of the 'newborn' small-scale island (along x) is of the

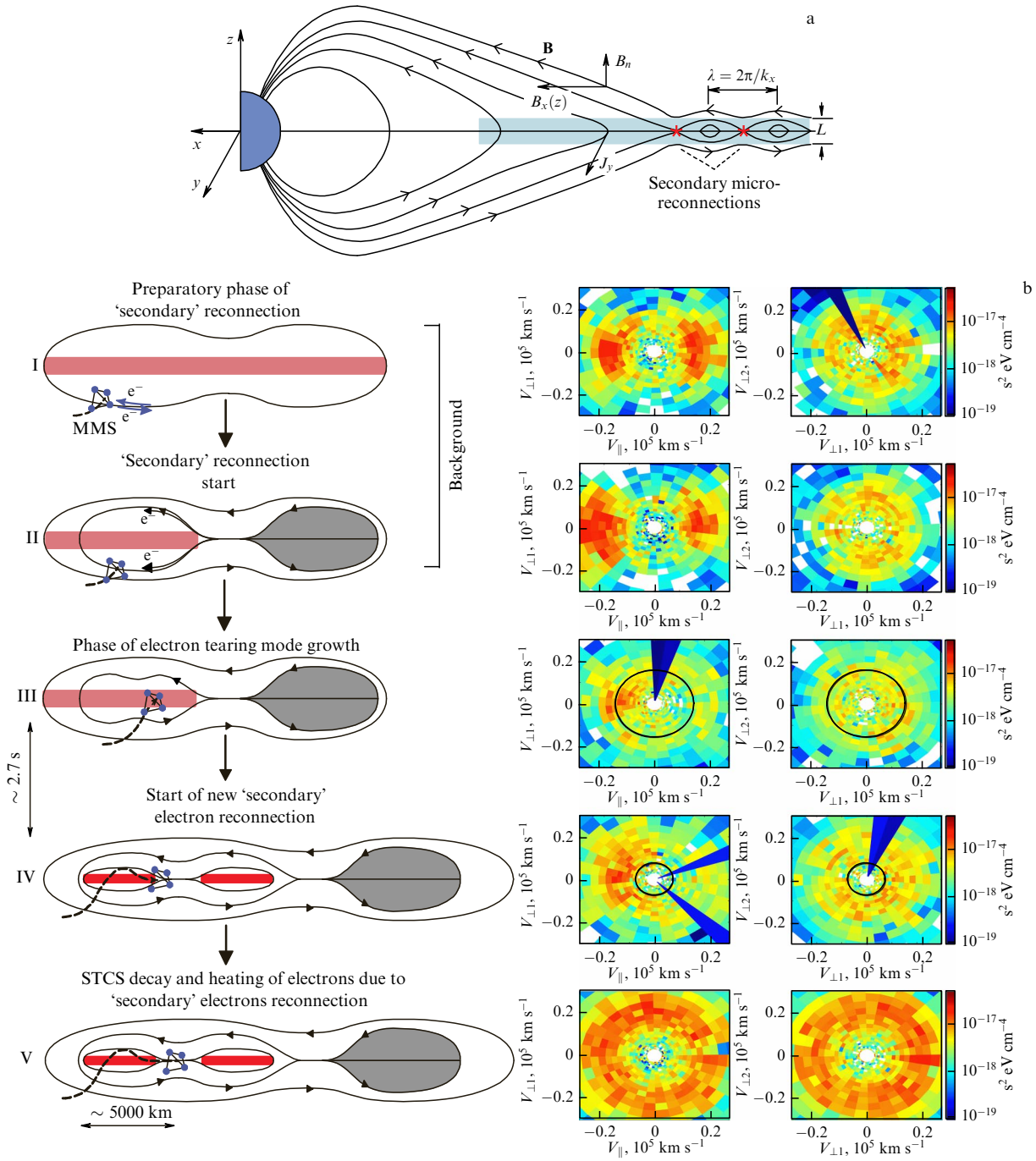

Figure 16. (a) Schematic of magnetic configuration of tail with magnetic islands formed as a result of development of electron tearing mode. (b) Scenario of evolution (fragmentation) of magnetic island as a result of development of electron tearing mode in STCS inside island. In left part of the figure, STCS is shown as a red rectangle. Evolution stages are presented for five time points, marked by vertical dashed lines in Fig. 15. Right part of figure shows corresponding 2D electron velocity distribution functions measured by MMS-1 satellite at indicated time points. Color scale on right corresponds to measurements of spectral density of electron velocity distribution. (Adapted from [184].)

order of $L \sim \sum_{t_1}^{t_2} v_{ix}(t)\Delta t \sim$ 4000–5500 km, where v_{ix} is the x component of the ion flow velocity, and t_1 and t_2 are the instants of observation of the island boundaries (observation of bipolar B_z variations). A change in the magnetic configuration associated with island fragmentation can cause the generation of induction electric fields, which in turn accelerates the new electron beam. Unfortunately, MMS observations do not allow observing all the relations in this chain of events. At instant V, the satellites were still near the neutral plane in the region between the 'newborn' islands, where the secondary reconnection process had apparently already been completed. In this region, the intense STCS had already decayed, resulting in strong thermalization and isotropization of the electron distribution function (see the electron distribution function observed at instant V in Fig. 16b). Indeed, after 16:01:30 UT, no current density bursts with an amplitude exceeding 30 nA m^{-2} were observed. Instead, a quasistationary current with a density $J_y \sim 10$ nA m^{-2}, typical of an ion-scale TCS, was present near the neutral plane (Fig. 15b).

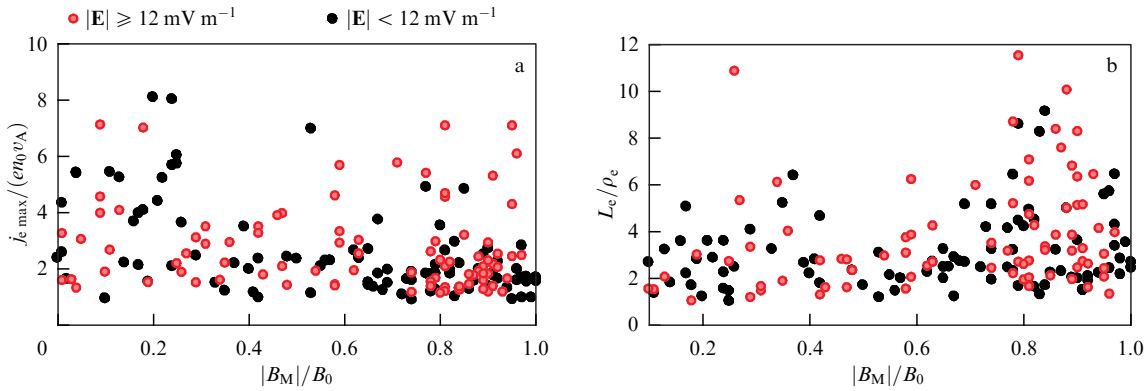

Figure 17. Scatter of (a) intensities j_e/en_0v_A and (b) half-thicknesses L_e/ρ_e of observed STCSs as a function of $|B_M|/B_0$. Observed STCSs are characterized by electric fields in range from 1.2 to 90 mV m^{-1}. Black and red dots correspond to STCS with $|\mathbf{E}| < 12$ mV m^{-1} and $|\mathbf{E}| \geqslant 12$ mV m^{-1}.

Thus, the MMS observations are in qualitative agreement with the model of the electron tearing mode evolution. The observed characteristic time of STCS evolution with a half-thickness of $\sim$ 20–50 km agrees with the theoretical estimate of the characteristic time of the fast electron tearing mode evolution ($\sim$ 4.5 s) in a magnetic island with a radial size of $\sim$ 4000–5500 km. For example, for the magnetic field $B \sim 20$ nT in the tail lobes ($\omega_{ci} \sim 1.92$ rad s^{-1}) and the ion temperature $T_i = 5$ keV (where $v_{Ti} = 980$ km s^{-1} is the ion thermal velocity), the electron tearing increment is $\gamma/\omega_{ci} = 0.7$ and the characteristic instability development time is $2\pi/\gamma \sim$ 4.7 s. For $k_x\rho_i = 0.6$–0.8, the wavelength is $\lambda = 2\pi/k_x =$ 4010–5350 km, which agrees with the observed size of the magnetic island in the x direction. During the instability development time, the induced electric field $E_{1y} = -\gamma A_{iy} =$ 6.9 mV m^{-1} (with $A_{iy} \approx 0.5B_0\rho_i \exp(\gamma t + ik_x x)$, where B_0 is the absolute value of the magnetic field at the CS edges) can increase exponentially and reach the observed values of $\sim$ 10–20 mV m^{-1}. Thus, the growth rate of the fast electron tearing mode is large enough to destabilize the STCS on a time scale of a few seconds, while the development time of the ion tearing mode for the same local parameters is several minutes.

We note that the observations by the MMS mission on July 6, 2017 demonstrated the development of the electron tearing mode accompanied by the generation of induction electric fields and fragmentation of magnetic islands. This process has a cascade nature: large-scale structures are fragmented into smaller ones, which leads to additional heating of electrons and dissipation of magnetic energy, as shown in Fig. 16. In turn, the induction electric fields arising as a result of changes in the magnetic configuration are capable of accelerating new electron beams. For example, an induction electric field with the observed strength of $\sim$ 20 mV, arising as a result of the decay of an STCS with a thickness of 50–100 km, is capable of accelerating electrons to superthermal energies ($\sim$ 1–2 keV). Such energies correspond to those of the current-carrying electron component in the STCS.

These observations confirm that the rapidly changing phenomena occurring on small scales are quite consistent with Syrovatskii's concept of dynamical CSs [14–16] and demonstrate a similarity with the mechanism of heating the solar corona through a cascade of small-scale reconnections, emphasizing the key role of electron processes in such phenomena.

To conclude this section, we present the results of a brief statistical analysis of STCS parameters. Figure 17 shows the results of a statistical study of the parameters of the observed STCSs: the dependences of the maximum values of the current density and the thickness of the sheets on the relative value of the shear component of the magnetic field (B_M/B_0). The shear component (B_M in the local LMN coordinate system) is understood as the component of the magnetic field directed parallel or antiparallel to the direction of the current density in the sheet. The red dots mark instances of anomalously strong electric fields ($\geqslant 12$ mV m^{-1}), an order of magnitude higher than typical values in the magnetosphere (usually, fractions of a mV m^{-1}). For quasistationary CSs, there is an increase in the thickness and a decrease in the current density with increasing magnetic shear in the sheet [76, 77]. But such a dependence is not observed for many STCSs. In particular, a significant number of STCSs from our database have a fairly high current density and small thickness at high B_M/B_0 values. Most of these STCSs were observed to have strong electric fields, indicating that the sheet is nonstationary. Our studies convincingly prove the vortex nature of these fields. These observations allow us to draw fundamentally important conclusions about the nature of STCSs:

- the sheets demonstrate a dynamical character, constantly evolving in the birth–decay cycle;
- the process is cascade in nature: the decaying sheets initiate the formation of new structures;
- the accompanying process bursts of vortex fields effectively accelerate electrons;
- the ion component remains practically unaffected due to its inertial nature.

The obtained results are remarkably similar to the theoretical work of Syrovatskii, who predicted the fundamental nonstationarity of reconnection processes in real plasma and the cascade nature of energy conversion.

5. Conclusions

The competition between two scientific schools, the Western school of Petschek and the Eastern school of Syrovatskii, which unfolded in the 1970s, opened up new perspectives for space scientists in the study of dynamical processes in space. Due to spacecraft and multisatellite missions such as ISEE-1–3, AMPTE, Interball, Cluster, MMS, and THEMIS, extremely thin CSs were discovered and studied; these

structures had long (for decades) been considered infinitely thin MHD discontinuities where magnetic reconnection processes occur.

It turns out that such structures have a finite thickness and can be studied using high-resolution multisatellite measurements with spacecraft located at distances of the order of ion or electron scales, from 10 to several thousand kilometers. From a theoretical standpoint, such CSs can be studied exclusively in the framework of kinetic or hybrid models. The MHD approximation is inapplicable to them. A breakthrough event in space physics was the discovery of ion-scale TCSs in the 1990s, which later began to be found everywhere in near-Earth space: on shock waves, at the magnetopause, in Earth's magnetotail, in polar cusps, and in the magnetospheres of other planets. TCSs can be classified as a class of surface boundary structures separating regions containing plasma with different properties and/or magnetic fields with different directions. The struggle of scientists to 'unfreeze' the ion tearing mode in Earth's magnetotail ultimately ran into the problem of a lack of a suitable thin CS model that would take the small but finite normal magnetic component in the tail into account. Such a model has been constructed and studied, and the ion tearing problem was thus solved [35, 45, 64, 67, 78]. It turns out that the characteristic property of TCSs in the tail was nesting, pressure anisotropy maintaining the balance, and the overall strong influence of the outer proton sheet on the electron CS nested inside it, which ultimately leads to metastability of the entire current configuration, when its stability is spontaneously interrupted by explosive destruction, energy release, and magnetic reconnection.

But progress in space science did not stop there. The new MMS space mission allowed discovering and describing STCSs, several ten kilometers thick, supported only by the electron population. Reconnection processes in them occurred continuously, mainly on the electron scale. Similar structures were observed throughout almost the entire thickness of the plasma sheet in the tail, mainly in the turbulence zone created by fast plasma flows.

Summarizing these observations, we can propose the following scenario of energy transformation in the plasma sheet of the geomagnetic tail. The primary macroreconnection accelerates the large-scale fast ion flow and generates magnetic structures of ion kinetic scales — dipolarization and antidipolarization fronts and magnetic islands [189–192], which move in the plasma sheet together with the fast flow. The fast ion flow thus transfers energy from the region of 'global' reconnection to distant parts of the plasma sheet. The fast flow moving with the flow velocity $\mathbf{V}_\mathrm{i}$ is associated with an increase in the convection electric field $\mathbf{E} = -[\mathbf{V}_\mathrm{i} \times \mathbf{B}]$, which is arguably a trigger for the rapid evolution of magnetic structures carried by the flow, accompanied by the generation of fairly strong induction electric fields. Such fields are capable of accelerating electron beams to superthermal energies. The emergence of this secondary accelerated electron population results in the emergence of STCSs, which are dynamical structures that eventually decay as a result of the development of the electron tearing mode, leading to secondary microreconnections. As a result of STCS decays, induction electric fields are generated again, accelerating new electron beams to energies of the order of several keV. The newly born electron beams, in turn, generate new STCSs, and this process continues wherever the primary fast ion flow propagates.

The accumulation of a vast amount of observational data on the structure and dynamics of STCSs gradually led to the need to organize the obtained data on superthin electron sheets and to try to understand which models can be used to describe individual groups of sheets from this entire rich spectrum of superthin current structures. In this review, we have attempted to formulate our standpoint on the accumulated array of data on thin and superthin sheets, which consists of dividing them into quasistationary and nonstationary structures, which allows them to be described in terms of the corresponding models of different classes with fundamentally different dynamically and spatial-structural characteristics.

In general, modern space observations agree with the dynamical nature of reconnection processes and the absence of stationary solutions predicted by Syrovatskii. Everything flows in nature, everything changes, and Syrovatskii's ideas live and develop.

The work of L.M. Zelenyi, E.E. Grigorenko, O.O. Tsareva, and M.V. Leonenko was carried out in the framework of the state program PLASMA. The work of H.V. Malova and V.Yu. Popov was supported by state programs of Lomonosov Moscow State University and PLASMA.

References

1. Parker E N *J. Geophys. Res.* **62** 509 (1957)
2. Sweet P A, in *Electromagnetic Phenomena in Cosmical Physics, Proc. IAU Symp. No. 6* Vol. 6 (Ed. B Lehnert) (Cambridge: Cambridge Univ. Press, 1958) p. 123
3. Parker E N *Astrophys. J. Suppl.* **8** 177 (1963)
4. Petschek H E, in *The Physics of Solar Flares, Proc. of the AAS–NASA Symp. 28–30 October, 1963, Greenbelt, MD* (NASA Special Publ., Vol. 50, Ed. W N Hess) (Washington, DC: National Aeronautics and Space Administration, Science and Technical Information Division, 1964) p. 425
5. Syrovatskii S I *Sov. Phys. Usp.* **14** 533 (1972); *Usp. Fiz. Nauk* **104** 669 (1971)
6. Syrovatskii S I *Sov. Phys. Usp.* **19** 354 (1976); *Usp. Fiz. Nauk* **118** 738 (1976)
7. Somov B V, Syrovatskii S I *Sov. Phys. Usp.* **19** 813 (1976); *Usp. Fiz. Nauk* **120** 217 (1976)
8. Kennel C F *Comments Astrophys. Space Phys.* **6** 71 (1975)
9. Alfvén H, Fälthammar C-G *Cosmic Electrodyn.* **2** 78 (1971)
10. Alfven H *J. Geophys. Res.* **81** 4019 (1976)
11. Giovanelli R G *Mon. Not. R. Astron. Soc.* **107** 338 (1947)
12. Dungey J W *Phys. Rev. Lett.* **6** 47 (1961)
13. Akasofu S-I *Planet. Space Sci.* **12** 573 (1964)
14. Syrovatskii S I *Usp. Fiz. Nauk* **62** 247 (1957)
15. Syrovatskii S I *Usp. Fiz. Nauk* **128** 380 (1979)
16. Kadomtsev B B *Usp. Fiz. Nauk* **151** 3 (1987); *Rep. Prog. Phys.* **50** 115 (1987)
17. Sato T *J. Geophys. Res.* **84** 7177 (1979)
18. Kowal G et al. *Astrophys. J.* **700** 63 (2009)
19. Zelenyi L M *Dinamika Plazmy i Magnitnykh Polei v Khvoste Magnitosfery Zemli* (Plasma and Magnetic Field Dynamics in the Earth's Magnetotail) (Results of Science and Technology. Ser. Space Exploration, Vol. 24) (Moscow: VINITI, 1986)
20. Pudovkin M I, Semenov V S *Space Sci. Rev.* **41** 1 (1985)
21. Bezrodnykh S I, Somov B V, Vlasov V I *Astron. Lett.* **37** 113 (2011); *Pis'ma Astron. Zh.* **37** 133 (2011)
22. Artemyev A V et al. *Ann. Geophys.* **27** 4075 (2009)
23. McPherron R L et al., in *Quantitative Modeling of Magnetosphere-Ionosphere Coupling Processes* (Eds Y Kamide, R A Wolf) (Kyoto: Kyoto Sangyo Univ., 1987) p. 252
24. Runov A, Nakamura R, Baumjohann W *Adv. Space Res.* **38** 85 (2006)
25. Frank A G *Phys. Usp.* **53** 941 (2010); *Usp. Fiz. Nauk* **180** 982 (2010)
26. Zelenyi L et al. *Plasma Phys. Control. Fusion* **58** 054002 (2016)

27. Frank A G et al. *Plasma Phys. Control. Fusion* **65** 095006 (2023)
28. Syrovatskii S I *Vestn. Akad. Nauk SSSR* (10) 33 (1977)
29. Syrovatskii S I *Priroda* (2) 143 (1978)
30. Syrovatskii S I *Annu. Rev. Astron. Astrophys.* **19** 163 (1981)
31. Biskamp D *Nonlinear Magnetohydrodynamics* (Cambridge: Cambridge Univ. Press, 1997)
32. Biskamp D, Schwarz E *Phys. Plasmas* **8** 4729 (2001)
33. Biskamp D, in *Energy Conversion and Particle Acceleration in the Solar Corona* (Lecture Notes in Physics, Vol. 612, Ed. K-L Klein) (Berlin: Springer, 2003) p. 109, https://doi.org/10.1007/3-540-36242-8_8
34. Ginzburg V L, Syrovatskii S I *Sov. Phys. Usp.* **3** 504 (1961); *Usp. Fiz. Nauk* **71** 411 (1960)
35. Zelenyi L M et al. *Plasma Phys. Rep.* **37** 118 (2011); *Fiz. Plazmy* **37** 137 (2011)
36. Ness N F *J. Geophys. Res.* **70** 2989 (1965)
37. Zelenyi L M, Milovanov A V *Phys. Usp.* **47** 749 (2004); *Usp. Fiz. Nauk* **174** 809 (2004)
38. Axford W I, Hines C O, in *The Upper Atmosphere in Motion* (Geophysical Monograph Series, No. 18, Ed. C O Hines) (Washington, DC: American Geophysical Union, 1974) p. 933
39. Feldstein Y I et al. *J. Atmos. Solar-Terr. Phys.* **65** 429 (2003)
40. Alexeev I I *Space Sci. Rev.* **107** 141 (2003)
41. Nagai T, Shinohara I *J. Geophys. Res.* **127** e30653 (2022)
42. Hones E W (Jr.), in *Magnetic Reconnection in Space and Laboratory Plasmas* (Geophysical Monograph, Vol. 30, Ed. E W Hones (Jr.)) (Washington, DC: American Geophysical Union, 1984) p. 178
43. Rostoker G et al. *Space Sci. Rev.* **46** 93 (1988)
44. Krymskii P F, Romashchenko I A *Geomagn. Aeron.* **30** 927 (1990)
45. Zelenyi L M et al. *Plasma Phys. Rep.* **47** 857 (2021); *Fiz. Plazmy* **47** 771 (2021)
46. Zelenyi L, Sauvaud J-A *Ann. Geophys.* **15** 511 (1997)
47. Zelenyi L, Sauvaud J-A *Ann. Geophys.* **20** 289 (2002)
48. Escoubet C P, Schmidt R, Goldstein M L *Space Sci. Rev.* **79** 11 (1997)
49. Runov A et al. *Geophys. Res. Lett.* **30** 1579 (2003)
50. Grigorenko E E, Sauvaud J-A, Zelenyi L M *J. Geophys. Res.* **112** A05218 (2007)
51. Vaivads A, Retinò A, André M *Space Sci. Rev.* **122** 19 (2006)
52. Fairfield D H, in *Magnetic Reconnection in Space and Laboratory Plasmas* (Geophysical Monograph, Vol. 30, Ed. E W Hones (Jr.)) (Washington, DC: American Geophysical Union, 1984) p. 168
53. Kaufmann R L *J. Geophys. Res.* **92** 7471 (1987)
54. Petrukovich A A et al. *J. Geophys. Res.* **112** A10213 (2007)
55. Mitchell D G et al. *Geophys. Res. Lett.* **17** 583 (1990)
56. Lui A T Y et al. *J. Geophys. Res.* **97** 1461 (1992)
57. Sergeev V A et al. *J. Geophys. Res.* **98** 17345 (1993)
58. Baker D N et al. *J. Geophys. Res.* **101** 12975 (1996)
59. Sanny J et al. *J. Geophys. Res.* **99** 5805 (1994)
60. Pulkkinen T I et al. *J. Geophys. Res.* **99** 5793 (1994)
61. Petrukovich A A et al. *J. Geophys. Res.* **116** A00I25 (2011)
62. Pulkkinen T I et al. *Geophys. Res. Lett.* **20** 2427 (1993)
63. Angelopoulos V et al. *Science* **321** 931 (2008)
64. Malova H V et al. *Astrophys. J.* **834** 34 (2017)
65. Guo A et al. *Astrophys. J.* **955** 14 (2023)
66. Panov E V et al. *Adv. Space Res.* **37** 1363 (2006)
67. Birn J, Hesse M *J. Geophys. Res.* **119** 290 (2014)
68. Zelenyi L et al. *Space Sci. Rev.* **132** 593 (2007)
69. Grigorenko E E et al. *J. Geophys. Res.* **122** 10176 (2017)
70. Artemyev A V, Vasko I Y, Kasahara S *Planet. Space Sci.* **96** 133 (2014)
71. Runov A et al. *Ann. Geophys.* **23** 1391 (2005)
72. Nakamura R et al. *Space Sci. Rev.* **122** 29 (2006)
73. Zelenyi L M et al. *Adv. Space Res.* **30** 1629 (2002)
74. Zelenyi L M et al. *Cosmic Res.* **40** 357 (2002); *Kosm. Issled.* **40** 385 (2002)
75. Malova H V et al. *Geophys. Res. Lett.* **34** L16108 (2007)
76. Kamaletdinov S R et al. *J. Geophys. Res.* **129** e2023JA032130 (2024)
77. Mingalev O V et al. *Plasma Phys. Rep.* **38** 300 (2012); *Fiz. Plazmy* **38** 329 (2012)
78. Zelenyi L M et al. *Nonlin. Processes Geophys.* **11** 579 (2004)
79. Zelenyi L M et al. *Geophys. Res. Lett.* **33** L05105 (2006)
80. Mingalev O V et al. *Plasma Phys. Rep.* **33** 942 (2007); *Fiz. Plazmy* **33** 1028 (2007)
81. Cowley S W H *J. Plasma Phys.* **12** 319 (1974)
82. Servidio S et al. *J. Geophys. Res.* **116** A09102 (2011)
83. Ledentsov L S, Somov B V *J. Exp. Theor. Phys.* **117** 1164 (2013); *Zh. Eksp. Teor. Fiz.* **144** 1319 (2013)
84. Malova H V et al. *J. Geophys. Res.* **120** 4802 (2015)
85. Manankova A V *Geomagn. Aeron.* **46** 322 (2006); *Geomagn. Aeron.* **46** 339 (2006)
86. Sitnov M I et al. *J. Geophys. Res.* **111** A08204 (2006)
87. Bykov A A, Zelenyi L M, Malova Kh V *Plasma Phys. Rep.* **34** 128 (2008); *Fiz. Plazmy* **34** 148 (2008)
88. Malova H V et al. *J. Geophys. Res.* **118** 4308 (2013)
89. Harris E G *Nuovo Cimento* **23** 115 (1962)
90. Lembege B, Pellat R *Phys. Fluids* **25** 1995 (1982)
91. Zelenyi L M et al. *Phys. Usp.* **59** 1057 (2016); *Usp. Fiz. Nauk* **186** 1153 (2016)
92. Zelenyi L M et al. *Phys. Usp.* **53** 933 (2010); *Usp. Fiz. Nauk* **180** 973 (2010)
93. Gontikakis C et al. *Astrophys. J.* **771** 126 (2013)
94. Sitnov M I et al. *J. Geophys. Res.* **105** 13029 (2000)
95. Zelenyi L M et al. *Nonlin. Processes Geophys.* **7** 127 (2000)
96. Tsyganenko N A, Mukai T *J. Geophys. Res.* **108** 1136 (2003)
97. Galeev A A, Zelenyi L M *Sov. Phys. JETP* **43** 1113 (1976); *Zh. Eksp. Teor. Fiz.* **70** 2133 (1976)
98. Zelenyi L et al. *J. Atmos. Solar-Terr. Phys.* **70** 325 (2008)
99. Speiser T W *J. Geophys. Res.* **70** 4219 (1965)
100. Eastwood J W *Planet. Space Sci.* **20** 1555 (1972)
101. Ashour-Abdalla M et al. *J. Geophys. Res.* **99** 14891 (1994)
102. Delcourt D C, Malova H V, Zelenyi L M *Geophys. Res. Lett.* **33** L06106 (2006)
103. Hoshino M et al. *J. Geophys. Res.* **103** 4509 (1998)
104. Mingalev O V et al. *Solar-Terr. Phys.* **7** (2) 11 (2021); *Solnechno-zemnaya Fiz.* **7** (2) 12 (2021)
105. Mingalev O V et al. *Plasma Phys. Rep.* **35** 76 (2009); *Fiz. Plazmy* **35** 85 (2009)
106. Malova H V et al. *J. Geophys. Res.* **117** A04212 (2012)
107. Sergeev V et al. *Geophys. Res. Lett.* **30** 1327 (2003)
108. Somov B V, Verneta A I *Space Sci. Rev.* **65** 253 (1993)
109. Wu M et al. *J. Geophys. Res.* **121** 7817 (2016)
110. Sitnov M et al. *Space Sci. Rev.* **215** 31 (2019)
111. Birn J et al. *Phys. Plasmas* **18** 111202 (2011)
112. Gonzalez W D et al., in *Magnetic Reconnection: Concepts and Applications* (Astrophysics and Space Science Library, Vol. 427, Eds W Gonzalez, E Parker) (Cham: Springer, 2016) p. 1, https://doi.org/10.1007/978-3-319-26432-5_1
113. Sitnov M I et al. *Geophys. Res. Lett.* **48** e93065 (2021)
114. Liu Y-H et al. *J. Geophys. Res.* **119** 9773 (2014)
115. Coppi B, Laval G, Pellat R *Phys. Rev. Lett.* **16** 1207 (1966)
116. Coroniti F V *Phys. Rev. Lett.* **38** 1355 (1977)
117. Schindler K *Space Sci. Rev.* **23** 365 (1979)
118. Esarey E, Molvig K *Geophys. Res. Lett.* **14** 367 (1987)
119. Galeev A A, in *Basic Plasma Physics* Vol. 1 (Eds A A Galeev, R N Sudan) (Amsterdam: North-Holland, 1983); *Osnovy Fiziki Plazmy* Vol. 1 (Eds A A Galeev, R Sudan) (Moscow: Energoizdat, 1983) in Russian
120. Büchner J, Zelenyi L M *J. Geophys. Res.* **94** 11821 (1989)
121. Malova H V, Sitnov M I *Phys. Lett. A* **177** 235 (1993)
122. Daughton W *Phys. Plasmas* **6** 1329 (1999)
123. Daughton W, Lapenta G, Ricci P *Phys. Rev. Lett.* **93** 105004 (2004)
124. Sitnov M I, Malova H V, Sharma A S *Geophys. Res. Lett.* **25** 269 (1998)
125. Sitnov M I, Malova H V, Sharma A S *Plasma Phys. Rep.* **25** 227 (1999); *Fiz. Plazmy* **25** 253 (1999)
126. Sitnov M I, Lui A T Y *J. Geophys. Res.* **104** 6941 (1999)
127. Büchner J *Adv. Space Res.* **18** 267 (1996)
128. Tsurutani B T et al. *Earth Planets Space* **61** 555 (2009)
129. Fairfield D H *J. Geophys. Res.* **97** 10865 (1992)
130. Sergeev V A, Pellinen R J, Pulkkinen T I *Space Sci. Rev.* **75** 551 (1996)
131. Pellat R, Coroniti F V, Pritchett P L *Geophys. Res. Lett.* **18** 143 (1991)

132. Malova Kh V et al. *Plasma Phys. Rep.* **36** 841 (2010); *Fiz. Plazmy* **36** 897 (2010)
133. Sagdeev R Z, Usikov D A, Zaslavsky G M *Nonlinear Physics*: *From the Pendulum to Turbulence and Chaos* (Chur: Harwood Acad. Publ., 1988); Zaslavsky G M, Sagdeev R Z *Vvedenie v Nelineinuyu Fiziku*: *Ot Mayatnika do Turbulentnosti i Khaosa* (Moscow: Nauka, 1988) in Russian
134. Sonnerup B U Ö *J. Geophys. Res.* **76** 8211 (1971)
135. Zelenyi L M et al. *Phys. Usp.* **56** 347 (2013); *Usp. Fiz. Nauk* **183** 365 (2013)
136. Chen J, Palmadesso P J *J. Geophys. Res.* **91** 1499 (1986)
137. Chen J *J. Geophys. Res.* **97** 15011 (1992)
138. Schindler K, in *Earth's Magnetospheric Processes. Proc. of a Symp., and 9th ESRO, European Space Research Organization, Summer School, Cortina, Italy, August 30 – September 10, 1971* (Astrophysics and Space Science Library, Vol. 32, Ed. B M McCormac) (Dordrecht: D. Reidel, 1972) p. 200
139. Zwingmann W *J. Geophys. Res.* **88** 9101 (1983)
140. Schindler K *Astrophys. Space Sci.* **264** 289 (1998)
141. Schindler K, Birn J *J. Geophys. Res.* **107** 1193 (2002)
142. Hill T W *J. Geophys. Res.* **80** 4689 (1975)
143. Francfort P, Pellat R *Geophys. Res. Lett.* **3** 433 (1976)
144. Pritchett P L, Coroniti F V *J. Geophys. Res.* **97** 16773 (1992)
145. Kropotkin A P, Domrin V I *J. Geophys. Res.* **101** 19893 (1996)
146. Kropotkin A P, Malova H V, Sitnov M I *J. Geophys. Res.* **102** 22099 (1997)
147. Birn J *J. Geophys. Res.* **85** 1214 (1980)
148. Kan J R *J. Geophys. Res.* **103** 11787 (1998)
149. Burkhart G R et al. *J. Geophys. Res.* **97** 13799 (1992)
150. Zelenyi L M et al., in *Multiscale Processes in the Earth's Magnetosphere*: *From Interball to Cluster* (NATO Science Ser. II, Vol. 178, Eds J-A Sauvaud, Z Němeček) (Dordrecht: Springer, 2004) p. 275, https://doi.org/10.1007/1-4020-2768-0_15
151. Zelenyi L M et al. *Geophys. Res. Lett.* **47** e2020GL088422 (2020)
152. Zelenyi L M et al. *J. Geophys. Res.* **127** e2022JA030881 (2022)
153. Khabarova O et al. *Space Sci. Rev.* **217** 38 (2021)
154. Pezzi O et al. *Space Sci. Rev.* **217** 39 (2021)
155. Ohtani S *Space Sci. Rev.* **95** 347 (2001)
156. Hwang K-J et al. *J. Geophys. Res.* **116** A00I32 (2011)
157. Nishimura Y et al. *J. Geophys. Res.* **129** e2024jA032924 (2024)
158. Ge Y S et al. *J. Geophys. Res.* **117** A10226 (2012)
159. Belehaki A et al. *Ann. Geophys.* **13** 494 (1995)
160. Zelenyi L M et al. *Cosmic Res.* **47** 352 (2009); *Kosm. Issled.* **47** 388 (2009)
161. Burch J L et al. *Space Sci. Rev.* **199** 5 (2016)
162. Wang R et al. *Geophys. Res. Lett.* **45** 4542 (2018)
163. Phan T D et al. *Geophys. Res. Lett.* **43** 6060 (2016)
164. Zhou M et al. *Phys. Rev. Lett.* **119** 055101 (2017)
165. Gingell I et al. *Geophys. Res. Lett.* **46** 1177 (2019)
166. Chen Z Z et al. *Geophys. Res. Lett.* **46** 10209 (2019)
167. Leonenko M V et al. *J. Geophys. Res.* **126** e2021JA029641 (2021)
168. Sonnerup B U Ö, Scheible M, in *Analysis Methods for Multi-Spacecraft Data* (ISSI Scientific Reports Ser., ESA/ISSI, Vol. 1, Eds G Paschmann, P Daly) (Frascati: ESA, 1998) p. 185
169. Grigorenko E E et al. *J. Geophys. Res.* **129** e2023JA032318 (2024)
170. Khabarova O et al. *Astrophys. J.* **933** 97 (2022)
171. Fu H S et al. *Geophys. Res. Lett.* **44** 37 (2017)
172. Huang S Y et al. *Geophys. Res. Lett.* **49** e2021GL096403 (2022)
173. Mallet A *J. Plasma Phys.* **86** 905860301 (2020)
174. Vega C et al. *Astrophys. J. Lett.* **893** L10 (2020)
175. Hubbert M et al. *J. Geophys. Res.* **127** e29584 (2022)
176. Man H Y et al. *Geophys. Res. Lett.* **45** 8729 (2018)
177. Poh G et al. *J. Geophys. Res.* **124** 7477 (2019)
178. Hesse M et al. *Space Sci. Rev.* **160** 3 (2011)
179. Torbert R B et al. *Science* **362** 1391 (2018)
180. Genestreti K J et al. *J. Geophys. Res.* **128** e2023JA031760 (2023)
181. Lu S et al. *Nat. Commun.* **11** 5049 (2020)
182. Lu S et al. *Astrophys. J.* **943** 100 (2023)
183. Huang S Y et al. *J. Geophys. Res.* **120** 6188 (2015)
184. Tsareva O O et al. *Geophys. Res. Lett.* **51** e2023GL106867 (2024)
185. Leonenko M V et al. *Atmosphere* **14** 722 (2023)
186. Tsareva O O et al. *J. Geophys. Res.* **128** e2023JA031459 (2023)
187. Büchner J, Zelenyi L M *Phys. Lett. A* **118** 395 (1986)
188. Alexeev I I, Kalegaev V V *J. Geophys. Res.* **100** 19267 (1995)
189. Runov A et al. *Geophys. Res. Lett.* **36** L14106 (2009)
190. Sitnov M I, Swisdak M, Divin A V *J. Geophys. Res.* **114** A04202 (2009)
191. Balikhin M A et al. *J. Geophys. Res.* **117** A08229 (2012)
192. Grigorenko E E et al. *J. Geophys. Res.* **119** 6553 (2014)